

---

# Object-aware Contrastive Learning for Debiased Scene Representation

---

Sangwoo Mo<sup>\*1</sup>, Hyunwoo Kang<sup>\*1</sup>, Kihyuk Sohn<sup>2</sup>, Chun-Liang Li<sup>2</sup>, Jinwoo Shin<sup>1</sup>

<sup>1</sup>KAIST <sup>2</sup>Google Cloud AI

{swmo, hyunwookang, jinwoos}@kaist.ac.kr, {kihyuks, chunliang}@google.com

## Abstract

Contrastive self-supervised learning has shown impressive results in learning visual representations from unlabeled images by enforcing invariance against different data augmentations. However, the learned representations are often contextually biased to the spurious scene correlations of different objects or object and background, which may harm their generalization on the downstream tasks. To tackle the issue, we develop a novel object-aware contrastive learning framework that first (a) localizes objects in a self-supervised manner and then (b) debias scene correlations via appropriate data augmentations considering the inferred object locations. For (a), we propose the contrastive class activation map (ContraCAM), which finds the most discriminative regions (e.g., objects) in the image compared to the other images using the contrastively trained models. We further improve the ContraCAM to detect multiple objects and entire shapes via an iterative refinement procedure. For (b), we introduce two data augmentations based on ContraCAM, object-aware random crop and background mixup, which reduce contextual and background biases during contrastive self-supervised learning, respectively. Our experiments demonstrate the effectiveness of our representation learning framework, particularly when trained under multi-object images or evaluated under the background (and distribution) shifted images.<sup>1</sup>

## 1 Introduction

Self-supervised learning of visual representations from unlabeled images is a fundamental task of machine learning, which establishes various applications including object recognition [1, 2], reinforcement learning [3, 4], out-of-distribution detection [5, 6], and multimodal learning [7, 8]. Recently, contrastive learning [1, 2, 9–15] has shown remarkable advances along this line. The idea is to learn invariant representations by attracting the different views (e.g., augmentations) of the same instance (i.e., positives) while contrasting different instances (i.e., negatives).<sup>2</sup>

Despite the success of contrastive learning on various downstream tasks [16], they still suffer from the generalization issue due to the unique features of the training datasets [17–19] or the choice of data augmentations [19–21]. In particular, the co-occurrence of different objects and background in randomly cropped patches (i.e., positives) leads the model to suffer from the *scene bias*. For example, Figure 1a presents two types of the scene bias: the positive pairs contain different objects (e.g., giraffe and zebra), and the patches contain adjacent object and background (e.g., zebra and safari). Specifically, the co-occurrence of different objects is called contextual bias [22], and that of object and background is called background bias [23]. Attracting the patches in contrastive learning

---

<sup>\*</sup>Equal contribution.

<sup>1</sup>Code is available at <https://github.com/alinelab/occon>.

<sup>2</sup>Some recent works (e.g., [14, 15]) attract the positives without contrasting the negatives. While we mainly focus on contrastive learning with negatives, our method is also applicable to the positive-only methods.

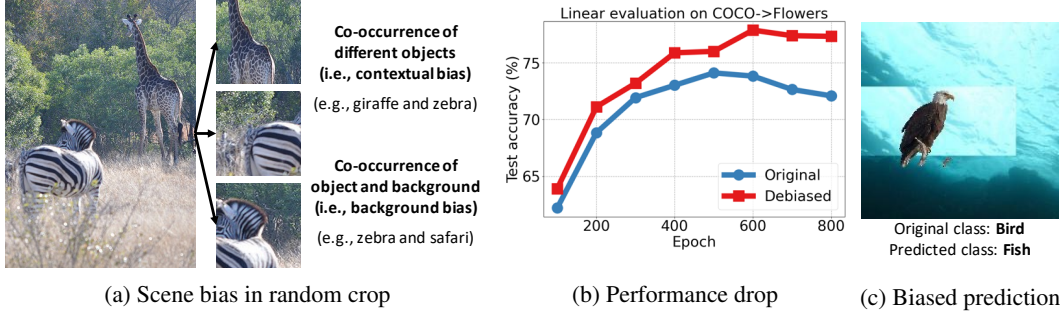


Figure 1: Scene bias issue (a) and its negative effects on contrastive learning. (b) Linear evaluation [24] of the original MoCov2 [1] and our debiased method, trained and evaluated on the COCO [25] and Flowers [26] datasets, respectively, using the ResNet-50 architecture [27]. (c) Biased prediction of MoCov2 and the original class on an image from the Background Challenge [23].

makes the features of correlated objects and background indistinguishable, which may harm their generalization (Figure 1b) because of being prone to biases (Figure 1c).

**Contribution.** We develop a novel object-aware contrastive learning framework that mitigates the scene bias and improves the generalization of learned representation. The key to success is the proposed *contrastive class activation map* (ContraCAM), a simple yet effective self-supervised object localization method by contrasting other images to find the most discriminate regions in the image. We leverage the ContraCAM to create new types of positives and negatives. First, we introduce two data augmentations for constructing the *positive* sample-pairs of contrastive learning: *object-aware random crop* and *background mixup* that reduce contextual and background biases, respectively. Second, by equipping ContraCAM with an iterative refinement procedure, we extend it to detect multiple objects and entire shapes, which allows us to generate masked images as effective *negatives*.

We demonstrate that the proposed method can improve two representative contrastive (or positive-only) representation learning schemes, MoCov2 [28] and BYOL [14], by reducing contextual and background biases as well as learning object-centric representation. In particular, we improve:

- The representation learning under multi-object images, evaluated on the COCO [25] dataset, boosting the performance on the downstream tasks, e.g., classification and detection.
- The generalizability of the learned representation on the background shifts, i.e., objects appear in the unusual background (e.g., fish on the ground), evaluated on the Background Challenge [23].
- The generalizability of the learned representation on the distribution shifts, particularly for the shape-biased, e.g., ImageNet-Sketch [29], and corrupted, e.g., ImageNet-C [30] datasets.

Furthermore, ContraCAM shows comparable results with the state-of-the-art unsupervised localization method (and also with the supervised classifier CAM) while being simple.

## 2 Object-aware Contrastive Learning

We first briefly review contrastive learning in Section 2.1. We then introduce our object localization and debiased contrastive learning methods in Section 2.2 and Section 2.3, respectively.

### 2.1 Contrastive learning

Contrastive self-supervised learning aims to learn an encoder  $f(\cdot)$  that extracts a useful representation from an unlabeled image  $x$  by attracting similar sample  $x^+$  (i.e., positives) and dispelling dissimilar samples  $\{x_i^-\}$  (i.e., negatives). In particular, instance discrimination [10] defines the same samples of different data augmentations (e.g., random crop) as the positives and different samples as negatives. Formally, contrastive learning maximizes the contrastive score:

$$s_{\text{con}}(x; x^+, \{x_n^-\}) := \log \frac{\exp(\text{sim}(z(x), \bar{z}(x^+))/\tau)}{\exp(\text{sim}(z(x), \bar{z}(x^+))/\tau) + \sum_{x_n^-} \exp(\text{sim}(z(x), \bar{z}(x_n^-))/\tau)}, \quad (1)$$

where  $z(\cdot)$  and  $\bar{z}(\cdot)$  are the output and target functions wrapping the representation  $f(x)$  for use,  $\text{sim}(\cdot, \cdot)$  denotes the cosine similarity, and  $\tau$  is a temperature hyperparameter. The specific form of  $z(\cdot)$ ,  $\bar{z}(\cdot)$  depends on the method. For example, MoCov2 [28] sets  $z(\cdot) = g(f(\cdot))$ ,  $\bar{z}(\cdot) = g_m(f_m(\cdot))$  where  $g(\cdot)$  is a projector network to indirectly match the feature  $f(x)$  and  $f_m(\cdot)$ ,  $g_m(\cdot)$  are the momentum version of the encoder and projectors. On the other hand, BYOL [14] sets  $z(\cdot) = h(g(f(\cdot)))$ ,  $\bar{z}(\cdot) = g_m(f_m(\cdot))$ , where  $h(\cdot)$  is an additional predictor network to avoid collapse of the features because it only maximizes the similarity score  $s_{\text{sim}}(x; x^+) := \text{sim}(z(x), \bar{z}(x^+))$  [14, 15].

**Scene bias in contrastive learning.** Despite the success of contrastive learning, they often suffer from the *scene bias*: entangling representations of co-occurring (but different) objects, i.e., contextual bias [22], or adjacent object and background, i.e., background bias [23], by attracting the randomly cropped patches reflecting the correlations (Figure 1a). The scene bias harms the performance (Figure 1b) and generalization of the learned representations on distribution shifts (Figure 1c). To tackle the issue, we propose object-aware data augmentations for debiased contrastive learning (Section 2.3) utilizing the object locations inferred from the contrastively trained models (Section 2.2).

## 2.2 ContraCAM: Unsupervised object localization via contrastive learning

We aim to find the most discriminative region in an image, such as objects for scene images, compared to the other images. To this end, we extend the (gradient-based) class activation map (CAM) [31, 32], originally used to find the salient regions for the prediction of classifiers. Our proposed method, *contrastive class activation map* (ContraCAM), has two differences from the classifier CAM. First, we use the contrastive score instead of the softmax probability. Second, we discard the negative signals from the similar objects in the negative batch since they cancel out the positive signals and hinder the localization, which is crucial as shown in Table 1 and Appendix C.1).

Following the classifier CAM, we define the saliency map as the weighted sum of spatial activations (e.g., penultimate feature before pooling), where the weight of each activation is given by the importance, the sum of gradients, of the activation for the score function. Formally, let  $\mathbf{A} := [A_{ij}^k]$  be a spatial activation of an image  $x$  where  $1 \leq i \leq H, 1 \leq j \leq W, 1 \leq k \leq K$  denote the index of row, column, and channel, and  $H, W, K$  denote the height, width, and channel size of the activation. Given a batch of samples  $\mathcal{B}$ , we define the score function of the sample  $x$  as the contrastive score  $s_{\text{con}}$  in Eq. (1) using the sample  $x$  itself as a positive<sup>3</sup> and the remaining samples  $\mathcal{B} \setminus x$  as negatives. Then, the weight of the  $k$ -th activation  $\alpha_k$  and the CAM mask  $\text{CAM} := [\text{CAM}_{ij}] \in [0, 1]^{H \times W}$  are:

$$\text{CAM}_{ij} = \text{Normalize} \left( \text{ReLU} \left( \sum_k \alpha_k A_{ij}^k \right) \right), \quad \alpha_k = \text{ReLU} \left( \frac{1}{HW} \sum_{i,j} \frac{\partial s_{\text{con}}(x; x, \mathcal{B} \setminus x)}{\partial A_{i,j}^k} \right), \quad (2)$$

where  $\text{Normalize}(x) := \frac{x - \min x}{\max x - \min x}$  is a normalization function that maps the elements to  $[0, 1]$ . We highlight the differences from the classifier CAM with the red color. Note that the ReLU used to compute  $\alpha_k$  in Eq. (2) discards the negative signals. The negative signal removal trick also slightly improves the classifier CAM [33] but much effective for the ContraCAM.

We further improve the ContraCAM to detect multiple objects and entire shapes with an iterative refinement procedure [34]: cover the salient regions of the image with the (reverse of) current CAM, predict new CAM from the masked image, and aggregate them (see Figure 2). It expands the CAM regions since the new CAM from the masked image detects the unmasked regions. Here, we additionally provide the masked images in the batch (parallelly computed) as the negatives: they are better negatives by removing the possibly existing similar objects. Also, we use the original image  $x$  as the positive to highlight the undetected objects. Formally, let  $\text{CAM}^t$  be the CAM of iteration  $t$  and  $\overline{\text{CAM}}^t := [\overline{\text{CAM}}_{ij}^t] = [\max_{l \leq t} \text{CAM}_{ij}^l]$  be the aggregated CAM mask. Also, let  $x^t$  be the image softly masked by the (reverse of) current aggregated mask, i.e.,  $x^t := (1 - \overline{\text{CAM}}^{t-1}) \odot x$  for  $t \geq 2$  and  $x^1 = x$  where  $\odot$  denotes an element-wise product, and  $\mathcal{B}^t := \{x_n^t\}$  be the batch of the masked images. Then, we define the score function for iteration  $t$  as:

$$s_{\text{con}}^t(x) := s_{\text{con}}(x^t; x, \cup_{l \leq t} (\mathcal{B}^l \setminus x^l)). \quad (3)$$

We substitute the contrastive score  $s_{\text{con}}$  in Eq. (2) with the  $s_{\text{con}}^t$  in Eq. (3) to compute the CAM of iteration  $t$ , and use the final aggregated mask after  $T$  iterations. We remark that the CAM results are

<sup>3</sup>It does not affect the score but is defined for the notation consistency with the iterative extension.

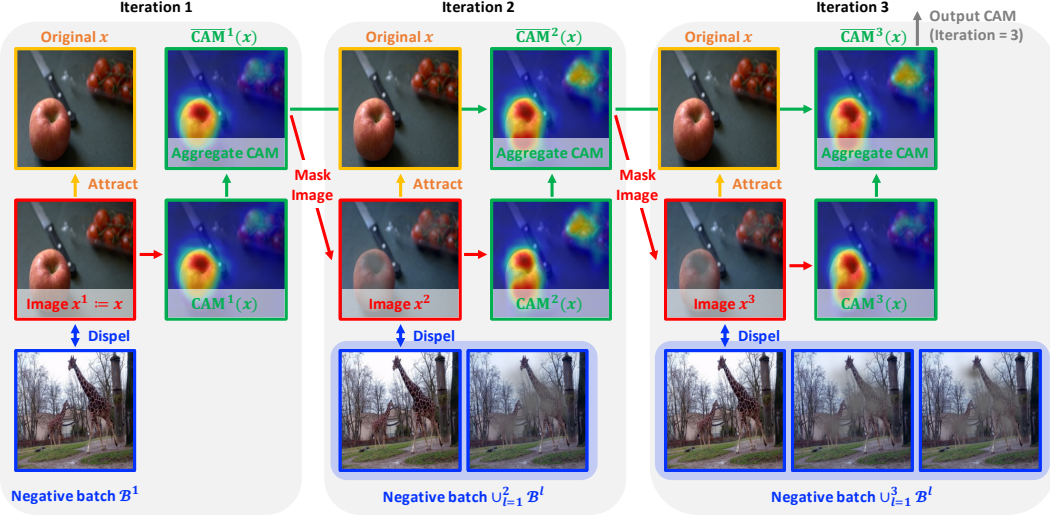


Figure 2: Visual illustration of the Iterative ContraCAM ( $T = 3$ ) procedure.

not sensitive to the number of iterations  $T$  if it is large enough; CAM converges to the stationary value since soft masking  $x^t$  regularizes the CAM not to be keep expanded (see Appendix C.2). We provide the pseudo-code of the entire Iterative ContraCAM procedure in Appendix A.

Note that contrastive learning was known to be ineffective at localizing objects [35] with standard saliency methods (using a classifier on top of the learned representation) since attracting the randomly cropped patches makes the model look at the entire scene. To our best knowledge, we are the first to extend the CAM for the self-supervised setting, relaxing the assumption of class labels. Selvaraju et al. [36] considered CAM for contrastive learning, but their purpose was to regularize CAM to be similar to the ground-truth masks (or predicted by pre-trained models) and used the similarity of the image and the masked image (by ground-truth masks) as the score function of CAM.

### 2.3 Object-aware augmentations for debiased contrastive learning

We propose two data augmentations for contrastive learning that reduce contextual and background biases, respectively, utilizing the object locations inferred by ContraCAM. Both augmentations are applied to the *positive* samples before other augmentations; thus, it is applicable for both contrastive learning (e.g., MoCov2 [28]) and positive-only methods (e.g., BYOL [14]).

**Reducing contextual bias.** We first tackle the contextual bias of contrastive learning, i.e., entangling the features of different objects. To tackle the issue, we propose a data augmentation named *object-aware random crop*, which restricts the random crop around a single object and avoids the attraction of different objects. To this end, we first extract the (possibly multiple or none) bounding boxes of the image from the binarized mask<sup>4</sup> of the ContraCAM. We then crop the image around the box, randomly chosen from the boxes, before applying other augmentations (e.g., random crop). Here, we apply augmentations (to produce positives) to the same cropped box; thus, the patches are restricted in the same box. Technically, it only requires a few line addition of code:

```

if len(boxes) > 0: # can be empty
    box = random.choice(boxes)
    image = image.crop(box)
# apply other augmentations (e.g., random crop)

```

Purushwalkam and Gupta [19] considered a similar approach using ground-truth bounding boxes applied on MoCov2. However, we found that cropping around the ground-truth boxes often harms contrastive learning (see Table 3). This is because some objects (e.g., small ones) in ground-truth boxes are hard to discriminate (as negatives), making contrastive learning hard to optimize. In contrast, the ContraCAM produces more discriminative boxes, often outperforming the ground-truth boxes

<sup>4</sup>Threshold the mask or apply a post-processing method, e.g., conditional random field (CRF) [37].

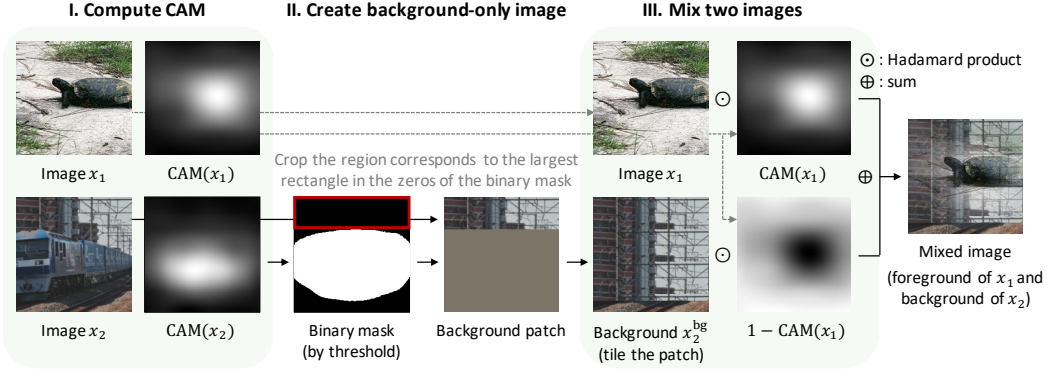


Figure 3: Visual illustration of the background mixup procedure.

(see Appendix D.1). Note that the positive-only methods do not suffer from the issue: both ground-truth and ContraCAM boxes work well. On the other hand, Selvaraju et al. [36] used a pre-trained segmentation model to constrain the patches to contain objects. It partly resolves the false positive issue by avoiding the attraction of background-only patches but does not prevent the patches with different objects; in contrast, the object-aware random crop avoids both cases.

**Reducing background bias.** We then tackle the background bias of contrastive learning, i.e., entangling the features of adjacent object and background. To this end, we propose a data augmentation named *background mixup*, which substitutes the background of an image with other backgrounds. Intuitively, the positive samples share the objects but have different backgrounds, thus reducing the background bias. Formally, background mixup blends an image  $x_1$  and a background-only image  $x_2^{\text{bg}}$  (generated from an image  $x_2$ ) using the ContraCAM of image  $x_1$  as a weight, i.e.,

$$x_1^{\text{bg-mix}} := \text{CAM}(x_1) \odot x_1 + (1 - \text{CAM}(x_1)) \odot x_2^{\text{bg}}, \quad (4)$$

where  $\odot$  denotes an element-wise product. Here, the background-only image  $x_2^{\text{bg}}$  is generated by tiling the background patch of the image  $x_2$  inferred by the ContraCAM. Precisely, we choose the largest rectangle in the zeros of the binarized CAM mask for the region of the background patch. The overall procedure of the background mixup is illustrated in Figure 3.

Prior works considered the background bias for contrastive learning [35, 38] but used a pre-trained segmentation model and copy-and-pasted the objects to the background-only images using binary masks. We also tested the copy-and-paste version with the binarized CAM, but the soft version in Eq. (4) performed better (see Appendix E.1); one should consider the confidence of the soft masks since they are inaccurate. Furthermore, the background mixup improves the generalization on distribution shifts, e.g., shape-biased [29, 39, 40] and corrupted [30] datasets (see Table 6). Remark that the background mixup often outperforms the Mixup [41] and CutMix [42] applied for contrastive learning [43]. Intuitively, the background mixup can be viewed as a saliency-guided extension [44, 45] of mixup but not mixing the targets (positives), since the mixed patch should be only considered as the positive of the patch sharing foreground, not the one sharing background.

### 3 Experiments

We first verify the localization performance of ContraCAM in Section 3.1. We then demonstrate the efficacy of our debiased contrastive learning: object-aware random crop improves the training under multi-object images by reducing contextual bias in Section 3.2, and background mixup improves generalization on background and distribution shifts by reducing background bias in Section 3.3.

**Common setup.** We apply our method on two representative contrastive (or positive-only) learning models: MoCov2 [28] and BYOL [14], under the ResNet-18 and ResNet-50 architectures [27]. We train the models for 800 epochs on COCO [25] and ImageNet-9 [23], and 2,000 epochs on CUB [46] and Flowers [26] datasets with batch size 256. We first train the vanilla MoCov2 and BYOL on the training dataset and pre-compute the CAM masks (and corresponding bounding boxes) using the models. Then, we train our method from scratch using the fixed pre-computed masks (and boxes).

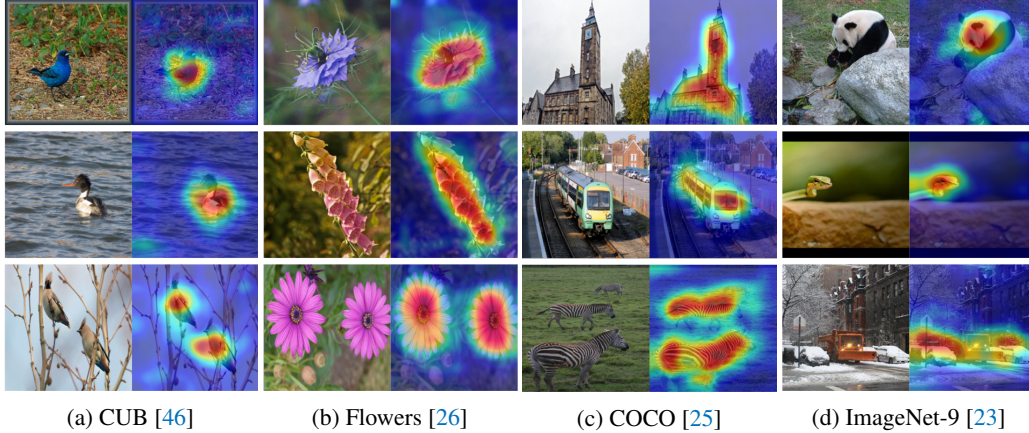


Figure 4: Visualization of the ContraCAM results on various image datasets.

Table 1: Mask mIoU of unsupervised object localization methods. Bold denotes the best results.

Method	CUB	Flowers	COCO	ImageNet-9
ReDO [50]	0.426	0.764	0.286	0.416
ContraCAM w/o negative signal removal	0.287	0.555	0.242	0.361
ContraCAM (ours)	<b>0.460</b>	<b>0.776</b>	<b>0.319</b>	<b>0.427</b>

Table 2: MaxBoxAccV2 of the classifier CAM and ContraCAM using the ImageNet-trained classifier and MoCov2. We report the localization results on the trained (ImageNet) and unseen datasets.

Model	Method	ImageNet	CUB	Flowers	VOC	OpenImages
Supervised	Classifier CAM	55.95	55.52	76.87	53.88	48.01
MoCov2	ContraCAM (ours)	55.88	64.07	75.64	59.40	49.89

We compute background-only images during training. We also retrained the model using the CAM masks inferred from our debiased model but did not see the gain (see Appendix D.4). We follow the default hyperparameters of MoCov2 and BYOL, except the smaller minimum random crop scale of 0.08 (instead of the original 0.2) since it performed better, especially for the multi-object images. We run a single trial for contextual bias and three trials for background bias experiments.

We use the penultimate spatial activations to compute the CAM results. At inference, we follow the protocol of [47] that doubly expands the resolution of the activations to detect the smaller objects through decreasing the stride of the convolutional layer in the final residual block. Since it produces the smaller masks, we use a larger number of iterations for the (Iterative) ContraCAM; specifically, we update ten iterations for object localization and contextual bias results. Here, we apply the conditional random field (CRF) using the default hyperparameters from the pydensecrf library [48] to produce segmentation masks and use the opencv [49] library to extract bounding boxes. We use a single iteration of the ContraCAM without the expansion trick for background bias results; it is sufficient for single instance images. Here, we binarize the masks with a threshold of 0.2 to produce background-only images. We provide the further implementation details in Appendix B.

**Computation time.** The training of the baseline models on the COCO ( $\sim 100,000$  samples) dataset takes  $\sim 1.5$  days on 4 GPUs and  $\sim 3$  days on 8 GPUs for ResNet-18 and ResNet-50 architectures, respectively, using a single machine with 8 GeForce RTX 2080 Ti GPUs; proportional to the number of samples and training epochs for other cases. The inference of ContraCAM takes a few minutes for the entire training dataset, and generating the boxes using CRF takes dozens of minutes. Using the pre-computed masks and boxes, our method only slightly increases the training time.

### 3.1 Unsupervised object localization

We check the performance of our proposed self-supervised object localization method, ContraCAM. Figure 4 shows the examples of the ContraCAM on various image datasets, including CUB, Flowers, COCO, and ImageNet-9 datasets. ContraCAM identifies the shapes of the objects and separates

Table 3: Linear evaluation (%) of MoCov2 and BYOL on various image classification tasks, trained with the original image (-) or object-aware random crop (OA-Crop) using the ContraCAM (CAM) or ground-truth (GT) bounding boxes from the COCO dataset. Gray lines denote the usage of GT boxes, blue and red brackets denote the gain and loss of OA-Crop compared to the original image.

Model	Network	OA-Crop	Test dataset						
			COCO-Crop	CIFAR10	CIFAR100	CUB	Flowers	Food	Pets
MoCov2	ResNet-50	-	74.30	77.58	53.26	22.90	72.09	59.70	59.25
MoCov2	ResNet-50	CAM	76.37 (+2.07)	84.10 (+6.52)	62.72 (+9.46)	25.46 (+2.56)	77.33 (+5.24)	62.01 (+2.31)	60.97 (+1.72)
MoCov2	ResNet-50	GT	76.44 (+2.14)	84.03 (+6.45)	62.81 (+9.55)	22.59 (-0.31)	75.09 (+3.00)	57.47 (-2.23)	57.67 (-1.58)
BYOL	ResNet-50	-	73.36	76.62	51.79	21.95	73.77	59.49	60.72
BYOL	ResNet-50	CAM	74.92 (+1.56)	82.79 (+6.17)	61.13 (+9.34)	24.34 (+2.39)	77.83 (+4.06)	61.83 (+2.34)	61.27 (+0.55)
BYOL	ResNet-50	GT	80.69 (+7.33)	85.92 (+9.30)	65.06 (+13.27)	28.68 (+6.73)	77.95 (+4.18)	64.63 (+5.14)	65.69 (+4.97)
MoCov2	ResNet-18	-	67.38	66.83	41.85	15.36	58.81	45.88	45.37
MoCov2	ResNet-18	CAM	69.92 (+2.54)	76.73 (+9.90)	53.25 (+11.40)	16.26 (+0.90)	64.77 (+5.96)	48.56 (+2.68)	47.37 (+2.00)
MoCov2	ResNet-18	GT	71.60 (+4.22)	77.99 (+11.16)	53.32 (+11.47)	18.19 (+2.83)	65.43 (+6.62)	46.41 (+0.53)	48.68 (+3.31)
BYOL	ResNet-18	-	67.74	67.82	41.96	17.24	64.79	49.58	52.90
BYOL	ResNet-18	CAM	70.85 (+3.11)	77.37 (+9.55)	54.79 (+12.83)	18.24 (+1.00)	70.56 (+5.77)	53.16 (+3.58)	54.27 (+1.37)
BYOL	ResNet-18	GT	76.59 (+8.85)	81.23 (+13.41)	58.11 (+16.15)	22.99 (+5.75)	73.25 (+8.46)	55.33 (+5.75)	59.80 (+6.90)

Table 4: Mean AP (%) of MoCov2 and BYOL fine-tuned on the COCO detection and segmentation tasks, following the setting of the table above, using the ResNet-50 architecture.

Dataset	MoCov2			BYOL		
	Baseline	OA-Crop (CAM)	OA-Crop (GT)	Baseline	OA-Crop (CAM)	OA-Crop (GT)
COCO Detection	36.34	36.60 (+0.26)	35.73 (-0.61)	35.11	35.63 (+0.52)	35.05 (-0.06)
COCO Segmentation	31.95	32.37 (+0.42)	31.47 (-0.48)	31.10	31.39 (+0.29)	31.12 (+0.02)

the different objects. We also provide the quantitative results in Table 1, reporting the mask mean intersection-over-unions (mIoUs). The ContraCAM is comparable with the state-of-the-art unsupervised object localization method, ReDO [50].<sup>5</sup> Also, one can see that the negative signal removal, i.e., ReLU in Eq. (1), is a critical to the performance (see Appendix C.1 for the visual examples).

We also compare the localization performance of the ContraCAM and the classifier CAM in Table 2, trained on the ImageNet [51] dataset under the ResNet-50 architecture, and evaluated on the trained (ImageNet) and unseen datasets. We use the publicly available supervised classifier [52] and MoCov2, and follow the MaxBoxAccV2 evaluation protocol [47] that averages the ratios of the bounding boxes whose mean intersection-over-unions (mIoUs) are larger than 30%, 50%, and 70%. The ContraCAM often outperforms the classifier CAM, especially for the unseen images (e.g., CUB). This is because the classifiers project the features unrelated to the target classes, losing their generalizability on the out-of-class samples. See Appendix C.4 for the detailed discussion.

We provide the additional analysis and results in Appendix C. It includes: effects of the number of iterations (Appendix C.2) and the choice of negative batches (Appendix C.3) for the ContraCAM, and comparison with the gradient-based saliency methods [53, 54] when used the same contrastive score (Appendix C.5). ContraCAM detects the background if we construct the batch with similar images, but providing a small amount of randomly selected images resolve the issue.

### 3.2 Reducing contextual bias: Representation learning from multi-object images

We demonstrate the effectiveness of the object-aware random crop (OA-Crop) for representation learning under multi-object images by reducing contextual bias. To this end, we train MoCov2 and BYOL on the COCO dataset, comparing them with the models that applied the OA-Crop using the ground-truth (GT) bounding boxes or inferred ones from the ContraCAM.

We first compare the linear evaluation [24], test accuracy of a linear classifier trained on top of the learned representation, in Table 3. We report the results on the COCO-Crop, i.e., the objects in the COCO dataset cropped by the GT boxes, CIFAR-10 and CIFAR-100 [55], CUB, Flowers, Food [56], and Pets [57] datasets. OA-Crop significantly improves the linear evaluation of MoCov2 and BYOL for all tested cases. Somewhat interestingly, OA-Crop using the ContraCAM boxes even

<sup>5</sup>We only consider fully self-supervised methods solely utilizing the data of the target domain.

Table 5: Test accuracy (%) of a linear classifier evaluated on the Background Challenge [23], both backbone and classifiers are trained under the ORIGINAL dataset. The backbone is trained from the original image (Baseline), background mixup using ContraCAM (BG-Mixup (CAM)), or hard background mixing using ground-truth masks (BG-HardMix (GT)), under the ResNet-18 architecture. Blue (or red) arrows imply higher (or lower) is better. Subscripts denote standard deviation.

Dataset	MoCov2			BYOL		
	Baseline	BG-Mixup (CAM)	BG-HardMix (GT)	Baseline	BG-Mixup (CAM)	BG-HardMix (GT)
Original $\uparrow$	89.17 $\pm$ 0.49	90.73 $\pm$ 0.05 (+1.56)	89.69 $\pm$ 0.14 (+0.52)	87.30 $\pm$ 0.61	89.30 $\pm$ 0.02 (+2.00)	90.95 $\pm$ 0.33 (+3.65)
Only-BG-B $\downarrow$	31.29 $\pm$ 2.46	29.60 $\pm$ 0.89 (-1.69)	26.44 $\pm$ 1.63 (-4.85)	25.59 $\pm$ 0.78	25.70 $\pm$ 3.46 (+0.11)	27.28 $\pm$ 0.04 (+1.69)
Only-BG-T $\downarrow$	44.91 $\pm$ 0.16	41.95 $\pm$ 0.38 (-2.96)	40.11 $\pm$ 0.58 (-4.80)	42.83 $\pm$ 0.51	39.94 $\pm$ 0.52 (-2.89)	41.16 $\pm$ 0.17 (-1.67)
Only-FG $\uparrow$	63.62 $\pm$ 4.71	70.55 $\pm$ 1.71 (+6.93)	72.68 $\pm$ 0.69 (+9.06)	61.04 $\pm$ 0.94	67.53 $\pm$ 0.30 (+6.49)	72.63 $\pm$ 1.13 (+11.59)
Mixed-Same $\uparrow$	80.98 $\pm$ 0.34	84.13 $\pm$ 0.33 (+3.15)	84.48 $\pm$ 0.17 (+3.50)	79.30 $\pm$ 0.31	81.28 $\pm$ 0.53 (+1.98)	84.94 $\pm$ 0.47 (+5.64)
Mixed-Rand $\uparrow$	60.34 $\pm$ 0.66	66.89 $\pm$ 0.54 (+6.55)	71.95 $\pm$ 0.54 (+11.61)	58.03 $\pm$ 0.85	63.83 $\pm$ 0.53 (+5.80)	70.51 $\pm$ 0.33 (+12.48)
Mixed-Next $\uparrow$	55.50 $\pm$ 0.71	63.64 $\pm$ 0.41 (+8.14)	70.25 $\pm$ 0.14 (+14.75)	53.35 $\pm$ 0.36	63.05 $\pm$ 3.54 (+9.70)	66.81 $\pm$ 0.08 (+13.46)
BG-Gap $\downarrow$	20.64 $\pm$ 0.36	17.24 $\pm$ 0.31 (-3.40)	12.53 $\pm$ 0.69 (-8.11)	21.27 $\pm$ 0.64	17.45 $\pm$ 0.15 (-3.82)	14.44 $\pm$ 0.56 (-6.83)

Table 6: Test accuracy (%) of a linear classifier evaluated on various distribution-shifted datasets, following the training of the table above, additionally comparing with Mixup [41] and CutMix [42].

Model	Augmentation	Test dataset			
		ImageNet-Sketch-9	Stylized-ImageNet-9	ImageNet-R-9	ImageNet-C-9
MoCov2	Baseline	46.70 $\pm$ 0.67	25.66 $\pm$ 0.54	37.51 $\pm$ 0.80	31.82 $\pm$ 0.40
MoCov2	+Mixup [41]	51.18 $\pm$ 0.88 (+4.48)	32.36 $\pm$ 0.12 (+6.70)	41.00 $\pm$ 0.12 (+3.49)	40.15 $\pm$ 2.07 (+8.33)
MoCov2	+CutMix [42]	45.92 $\pm$ 0.88 (-0.78)	26.46 $\pm$ 0.68 (+0.80)	37.07 $\pm$ 0.31 (-0.44)	32.29 $\pm$ 0.60 (+0.47)
MoCov2	+BG-Mixup (ours)	<b>52.15</b> $\pm$ 0.93 (+5.45)	<b>33.36</b> $\pm$ 0.61 (+7.70)	<b>41.50</b> $\pm$ 0.45 (+3.99)	<b>44.39</b> $\pm$ 0.89 (+12.57)
BYOL	Baseline	45.15 $\pm$ 1.12	23.80 $\pm$ 0.45	36.21 $\pm$ 0.31	28.62 $\pm$ 0.06
BYOL	+Mixup [41]	50.12 $\pm$ 1.61 (+1.97)	<b>28.11</b> $\pm$ 1.15 (+4.31)	37.90 $\pm$ 0.44 (+1.69)	32.48 $\pm$ 0.55 (+3.86)
BYOL	+CutMix [42]	46.07 $\pm$ 0.05 (+1.39)	23.98 $\pm$ 0.05 (+0.18)	35.43 $\pm$ 0.44 (-0.78)	29.68 $\pm$ 0.39 (+1.06)
BYOL	+BG-Mixup (ours)	<b>52.40</b> $\pm$ 0.70 (+7.25)	27.01 $\pm$ 0.74 (+3.21)	<b>39.62</b> $\pm$ 0.21 (+3.41)	<b>33.83</b> $\pm$ 0.28 (+5.21)

outperforms the GT boxes for MoCov2 under the ResNet-50 architecture. This is because the GT boxes often contain objects hard to discriminate (e.g., small objects), making contrastive learning hard to optimize; in contrast, ContraCAM finds more distinct objects. Note that BYOL does not suffer from this issue and performs well with both boxes. See Appendix D.1 for the detailed discussion.

We also compare the detection (and segmentation) performance measured by mean average precision (AP), an area under the precision-recall curve of the bounding boxes (or segmentation masks), on the COCO detection and segmentation tasks in Table 4. Here, we fine-tune the MoCov2 and BYOL models using the ResNet-50 architecture. Remark that OA-Crop using the ContraCAM boxes outperforms the baselines, while the GT boxes are on par or worse. This is because the GT boxes solely focus on the objects while ContraCAM also catches the salient scene information.

### 3.3 Reducing background bias: Generalization on background and distribution shifts

We demonstrate the effectiveness of the background mixup (BG-Mixup) for the generalization of the learned representations on background and distribution shifts by reducing background bias and learning object-centric representation. To this end, we train MoCov2 and BYOL (and BG-Mixup upon them) on the ORIGINAL dataset from the Background Challenge [23], a 9 superclass (370 classes) subset of the ImageNet [51]. We then train a linear classifier on top of the learned representation using the ORIGINAL dataset. Here, we evaluate the classifier on the Background Challenge datasets for the background shift results, and the corresponding 9 superclasses of the ImageNet-Sketch [29], Stylized-ImageNet [39], ImageNet-R [40], and ImageNet-C [30] datasets, denoted by putting ‘-9’ at the suffix of the dataset names, for the distribution shift results (see Appendix B.3 for details).

We additionally compare BG-Mixup with the hard background mixing (i.e., copy-and-paste) using ground-truth masks (BG-HardMix (GT)) for the background shift experiments, and Mixup [41] and CutMix [42] (following the training procedure of [43]) for the distribution shift experiments. We also tested the BG-HardMix using the binarized CAM but did not work well (see Appendix E.1). On the other hand, the BG-Mixup often makes contrastive learning hard to be optimized by producing hard positives; thus, we apply BG-Mix with probability  $p_{\text{mix}} < 1$ , independently applied on the patches. We tested  $p_{\text{mix}} \in \{0.2, 0.3, 0.4, 0.5\}$  and choose  $p_{\text{mix}} = 0.4$  for MoCov2 and  $p_{\text{mix}} = 0.3$  for BYOL.

Note that MoCov2 permits the higher  $p_{\text{mix}}$ , since finding the closest sample from the (finite) batch is easier than clustering infinitely many samples (see Appendix E.2 for details).

Table 5 presents the results on background shifts: BG-Mixup improves the predictions on the object-focused datasets (e.g., MIXED-RAND) while regularizing the background-focused datasets (e.g., ONLY-BG-T). Table 6 presents the results on distribution shifts: BG-Mixup mostly outperforms the Mixup and the CutMix. We also provide the BG-HardMix (GT) results on distribution shifts in Appendix E.3 and the mixup results on background shifts in Appendix E.4. The superiority of BG-Mix on both background and distribution shifts shows that its merits come from both object-centric learning via reducing background and the saliency-guided input interpolation.

## 4 Related work

**Contrastive learning.** Contrastive learning (or positive-only method) [1, 2, 14] is the state-of-the-art method for visual representation learning. However, they suffer from an inherent problem of matching false positives. We tackle this scene bias issue and improve the quality of learned representation. Note that prior work considering the scene bias for contrastive learning [19, 35, 36, 38] assumed ground-truth object annotations or pre-trained segmentation models, undermining the motivation of self-supervised learning to reduce such supervision. In contrast, we propose a fully self-supervised framework of object localization and debiased contrastive learning.

**Bias in visual representation.** The bias (or shortcut) in neural networks [58] have got a significant attention recently, pointing out the unintended over-reliance on, e.g., texture [39], background [23] or adversarial features [59]. Numerous works have thus attempted to remove such biases, particularly in an unsupervised manner, e.g., [29, 60, 61]. Our work also lies on this line: we raise a scene bias of contrastive (and positive-only) representation learning and a self-supervised way to fix it.

**Unsupervised object localization.** The deep-learning-based unsupervised object localization methods can be categorized as follow. (a) The generative-based [50, 62, 63] approaches train a generative model that disentangles the objects and background by enforcing the object-perturbed image to be considered as real. (b) The noisy-ensemble [64–66] approaches train a model using handcrafted predictions as noisy targets. Despite the training is unsupervised, they initialize the weights with the supervised model. (c) Voynov et al. [67] manually finds the ‘salient direction’ from the noise (latent) of the ImageNet-trained BigGAN [68]. Besides, scene decomposition (e.g., [69]) aims at a more ambitious goal: fully decompose the objects and background, but currently not scale to the complex images. To our best knowledge, the generative-based approach is the state-of-the-art method for fully unsupervised scenarios. Our proposed ContraCAM could be an alternative in this direction.

**Class activation map.** Class activation map [31, 32] has been used for the weakly-supervised object localization (WSOL), inferring the pixel- (or object-) level annotations using class labels. ContraCAM further expands its applicability by relaxing the requirements of class labels.

## 5 Conclusion and Discussion

We proposed the ContraCAM, a simple and effective self-supervised object localization method using the contrastively trained models. We then introduced two data augmentations upon the ContraCAM that reduce scene bias and improve the quality of the learned representations for contrastive learning. We remark that the scene bias is more severe for the uncurated images; our work would be a step towards strong self-supervised learning under real-world scenarios [70, 71].

**Limitations.** Since the ContraCAM finds the most salient regions, it can differ from the desiderata of the users, e.g., the ContraCAM detects both the birds and branches in the CUB [46] dataset, but one may only want to detect the birds. Also, though the ContraCAM identifies the disjoint objects, it is hard to separate the occluded objects. Incorporating the prior knowledge of the objects and designing a more careful method to disentangle objects would be an interesting future direction.

**Potential negative impacts.** Our proposed framework enforces the model to focus on the “objects”, or the salient regions, to disentangle the relations of the objects and background. However, ContraCAM may over-rely on the conspicuous objects and the derived data augmentation strategy by ContraCAM could potentially incur imbalanced performance across different objects. We remark that the biases in datasets and models cannot be entirely eliminated without carefully designed guidelines. While we empirically observe our proposed learning strategies mitigate contextual and background biases on certain object types, we still need a closer look at the models, interactively correcting them.

## Acknowledgements

We thank Jihoon Tack, Jongjin Park, and Sihyun Yu for their valuable feedback and comments.

## References

- [1] K. He, H. Fan, Y. Wu, S. Xie, and R. Girshick. Momentum contrast for unsupervised visual representation learning. In *IEEE Conference on Computer Vision and Pattern Recognition*, 2020.
- [2] T. Chen, S. Kornblith, M. Norouzi, and G. Hinton. A simple framework for contrastive learning of visual representations. In *International Conference on Machine Learning*, 2020.
- [3] A. Anand, E. Racah, S. Ozair, Y. Bengio, M.-A. Côté, and R. D. Hjelm. Unsupervised state representation learning in atari. In *Advances in Neural Information Processing Systems*, 2019.
- [4] A. Srinivas, M. Laskin, and P. Abbeel. Curl: Contrastive unsupervised representations for reinforcement learning. In *International Conference on Machine Learning*, 2020.
- [5] J. Tack, S. Mo, J. Jeong, and J. Shin. Csi: Novelty detection via contrastive learning on distributionally shifted instances. In *Advances in Neural Information Processing Systems*, 2020.
- [6] K. Sohn, C.-L. Li, J. Yoon, M. Jin, and T. Pfister. Learning and evaluating representations for deep one-class classification. In *International Conference on Learning Representations*, 2021.
- [7] A. Radford, J. W. Kim, C. Hallacy, A. Ramesh, G. Goh, S. Agarwal, G. Sastry, A. Askell, P. Mishkin, J. Clark, et al. Learning transferable visual models from natural language supervision. *arXiv preprint arXiv:2103.00020*, 2021.
- [8] T. Afouras, Y. M. Asano, F. Fagan, A. Vedaldi, and F. Metze. Self-supervised object detection from audio-visual correspondence. *arXiv preprint arXiv:2104.06401*, 2021.
- [9] A. v. d. Oord, Y. Li, and O. Vinyals. Representation learning with contrastive predictive coding. *arXiv preprint arXiv:1807.03748*, 2018.
- [10] Z. Wu, Y. Xiong, S. X. Yu, and D. Lin. Unsupervised feature learning via non-parametric instance discrimination. In *IEEE Conference on Computer Vision and Pattern Recognition*, 2018.
- [11] I. Misra and L. v. d. Maaten. Self-supervised learning of pretext-invariant representations. In *IEEE Conference on Computer Vision and Pattern Recognition*, 2020.
- [12] M. Caron, I. Misra, J. Mairal, P. Goyal, P. Bojanowski, and A. Joulin. Unsupervised learning of visual features by contrasting cluster assignments. In *Advances in Neural Information Processing Systems*, 2020.
- [13] Y. Tian, D. Krishnan, and P. Isola. Contrastive multiview coding. In *European Conference on Computer Vision*, 2020.
- [14] J.-B. Grill, F. Strub, F. Altché, C. Tallec, P. H. Richemond, E. Buchatskaya, C. Doersch, B. A. Pires, Z. D. Guo, M. G. Azar, et al. Bootstrap your own latent: A new approach to self-supervised learning. In *Advances in Neural Information Processing Systems*, 2020.
- [15] X. Chen and K. He. Exploring simple siamese representation learning. In *IEEE Conference on Computer Vision and Pattern Recognition*, 2021.
- [16] N. Zhao, Z. Wu, R. W. Lau, and S. Lin. What makes instance discrimination good for transfer learning? In *International Conference on Learning Representations*, 2021.
- [17] K. L. Hermann, T. Chen, and S. Kornblith. The origins and prevalence of texture bias in convolutional neural networks. In *Advances in Neural Information Processing Systems*, 2020.
- [18] R. Geirhos, K. Narayanappa, B. Mitzkus, M. Bethge, F. A. Wichmann, and W. Brendel. On the surprising similarities between supervised and self-supervised models. *arXiv preprint arXiv:2010.08377*, 2020.
- [19] S. Purushwalkam and A. Gupta. Demystifying contrastive self-supervised learning: Invariances, augmentations and dataset biases. In *Advances in Neural Information Processing Systems*, 2020.
- [20] Y. Tian, C. Sun, B. Poole, D. Krishnan, C. Schmid, and P. Isola. What makes for good views for contrastive learning. In *International Conference on Machine Learning*, 2020.
- [21] T. Xiao, X. Wang, A. A. Efros, and T. Darrell. What should not be contrastive in contrastive learning. In *International Conference on Learning Representations*, 2021.
- [22] K. K. Singh, D. Mahajan, K. Grauman, Y. J. Lee, M. Feiszli, and D. Ghahyaram. Don’t judge an object by its context: Learning to overcome contextual bias. In *IEEE Conference on Computer Vision and Pattern Recognition*, 2020.
- [23] K. Xiao, L. Engstrom, A. Ilyas, and A. Madry. Noise or signal: The role of image backgrounds in object recognition. In *International Conference on Learning Representations*, 2021.

- [24] A. Kolesnikov, X. Zhai, and L. Beyer. Revisiting self-supervised visual representation learning. In *IEEE Conference on Computer Vision and Pattern Recognition*, 2019.
- [25] T.-Y. Lin, M. Maire, S. Belongie, J. Hays, P. Perona, D. Ramanan, P. Dollár, and C. L. Zitnick. Microsoft coco: Common objects in context. In *European Conference on Computer Vision*, 2014.
- [26] M.-E. Nilsback and A. Zisserman. A visual vocabulary for flower classification. In *IEEE Conference on Computer Vision and Pattern Recognition*, 2006.
- [27] K. He, X. Zhang, S. Ren, and J. Sun. Deep residual learning for image recognition. In *IEEE Conference on Computer Vision and Pattern Recognition*, 2016.
- [28] X. Chen, H. Fan, R. Girshick, and K. He. Improved baselines with momentum contrastive learning. *arXiv preprint arXiv:2003.04297*, 2020.
- [29] H. Wang, S. Ge, Z. Lipton, and E. P. Xing. Learning robust global representations by penalizing local predictive power. In *Advances in Neural Information Processing Systems*, 2019.
- [30] D. Hendrycks and T. Dietterich. Benchmarking neural network robustness to common corruptions and perturbations. In *International Conference on Learning Representations*, 2019.
- [31] B. Zhou, A. Khosla, A. Lapedriza, A. Oliva, and A. Torralba. Learning deep features for discriminative localization. In *IEEE Conference on Computer Vision and Pattern Recognition*, 2016.
- [32] R. R. Selvaraju, M. Cogswell, A. Das, R. Vedantam, D. Parikh, and D. Batra. Grad-cam: Visual explanations from deep networks via gradient-based localization. In *IEEE International Conference on Computer Vision*, 2017.
- [33] W. Bae, J. Noh, and G. Kim. Rethinking class activation mapping for weakly supervised object localization. In *European Conference on Computer Vision*, 2020.
- [34] Y. Wei, J. Feng, X. Liang, M.-M. Cheng, Y. Zhao, and S. Yan. Object region mining with adversarial erasing: A simple classification to semantic segmentation approach. In *IEEE Conference on Computer Vision and Pattern Recognition*, 2017.
- [35] N. Zhao, Z. Wu, R. W. Lau, and S. Lin. Distilling localization for self-supervised representation learning. In *AAAI Conference on Artificial Intelligence*, 2021.
- [36] R. R. Selvaraju, K. Desai, J. Johnson, and N. Naik. Casting your model: Learning to localize improves self-supervised representations. In *IEEE Conference on Computer Vision and Pattern Recognition*, 2021.
- [37] J. Lafferty, A. McCallum, and F. C. Pereira. Conditional random fields: Probabilistic models for segmenting and labeling sequence data. In *International Conference on Machine Learning*, 2001.
- [38] C. K. Ryali, D. J. Schwab, and A. S. Morcos. Leveraging background augmentations to encourage semantic focus in self-supervised contrastive learning. *arXiv preprint arXiv:2103.12719*, 2021.
- [39] R. Geirhos, P. Rubisch, C. Michaelis, M. Bethge, F. A. Wichmann, and W. Brendel. Imagenet-trained cnns are biased towards texture; increasing shape bias improves accuracy and robustness. In *International Conference on Learning Representations*, 2019.
- [40] D. Hendrycks, S. Basart, N. Mu, S. Kadavath, F. Wang, E. Dorundo, R. Desai, T. Zhu, S. Parajuli, M. Guo, D. Song, J. Steinhardt, and J. Gilmer. The many faces of robustness: A critical analysis of out-of-distribution generalization. *arXiv preprint arXiv:2006.16241*, 2020.
- [41] H. Zhang, M. Cisse, Y. N. Dauphin, and D. Lopez-Paz. mixup: Beyond empirical risk minimization. In *International Conference on Learning Representations*, 2018.
- [42] S. Yun, D. Han, S. J. Oh, S. Chun, J. Choe, and Y. Yoo. Cutmix: Regularization strategy to train strong classifiers with localizable features. In *IEEE International Conference on Computer Vision*, 2019.
- [43] K. Lee, Y. Zhu, K. Sohn, C.-L. Li, J. Shin, and H. Lee. i-mix: A domain-agnostic strategy for contrastive representation learning. In *International Conference on Learning Representations*, 2021.
- [44] J.-H. Kim, W. Choo, and H. O. Song. Puzzle mix: Exploiting saliency and local statistics for optimal mixup. In *International Conference on Machine Learning*, 2020.
- [45] A. Uddin, M. Monira, W. Shin, T. Chung, S.-H. Bae, et al. Saliencymix: A saliency guided data augmentation strategy for better regularization. In *International Conference on Learning Representations*, 2021.
- [46] C. Wah, S. Branson, P. Welinder, P. Perona, and S. Belongie. The Caltech-UCSD Birds-200-2011 Dataset. Technical Report CNS-TR-2011-001, California Institute of Technology, 2011.
- [47] J. Choe, S. J. Oh, S. Lee, S. Chun, Z. Akata, and H. Shim. Evaluating weakly supervised object localization methods right. In *IEEE Conference on Computer Vision and Pattern Recognition*, 2020.
- [48] P. Krähenbühl and V. Koltun. Efficient inference in fully connected crfs with gaussian edge potentials. In *Advances in Neural Information Processing Systems*, 2011.

- [49] G. Bradski. The OpenCV Library. *Dr. Dobb's Journal of Software Tools*, 2000.
- [50] M. Chen, T. Artières, and L. Denoyer. Unsupervised object segmentation by redrawing. In *Advances in Neural Information Processing Systems*, 2019.
- [51] J. Deng, W. Dong, R. Socher, L.-J. Li, K. Li, and L. Fei-Fei. Imagenet: A large-scale hierarchical image database. In *IEEE Conference on Computer Vision and Pattern Recognition*, 2009.
- [52] A. Paszke, S. Gross, F. Massa, A. Lerer, J. Bradbury, G. Chanan, T. Killeen, Z. Lin, N. Gimelshein, L. Antiga, et al. Pytorch: An imperative style, high-performance deep learning library. *arXiv preprint arXiv:1912.01703*, 2019.
- [53] M. Sundararajan, A. Taly, and Q. Yan. Axiomatic attribution for deep networks. In *International Conference on Machine Learning*, 2017.
- [54] D. Smilkov, N. Thorat, B. Kim, F. Viégas, and M. Wattenberg. Smoothgrad: removing noise by adding noise. *arXiv preprint arXiv:1706.03825*, 2017.
- [55] A. Krizhevsky et al. Learning multiple layers of features from tiny images, 2009.
- [56] L. Bossard, M. Guillaumin, and L. Van Gool. Food-101—mining discriminative components with random forests. In *European Conference on Computer Vision*, 2014.
- [57] O. M. Parkhi, A. Vedaldi, A. Zisserman, and C. Jawahar. Cats and dogs. In *IEEE Conference on Computer Vision and Pattern Recognition*, 2012.
- [58] R. Geirhos, J.-H. Jacobsen, C. Michaelis, R. Zemel, W. Brendel, M. Bethge, and F. A. Wichmann. Shortcut learning in deep neural networks. *Nature Machine Intelligence*, 2020.
- [59] A. Ilyas, S. Santurkar, D. Tsipras, L. Engstrom, B. Tran, and A. Madry. Adversarial examples are not bugs, they are features. In *Advances in Neural Information Processing Systems*, 2019.
- [60] M. Minderer, O. Bachem, N. Houlsby, and M. Tschannen. Automatic shortcut removal for self-supervised representation learning. In *International Conference on Machine Learning*, 2020.
- [61] J. Nam, H. Cha, S. Ahn, J. Lee, and J. Shin. Learning from failure: Training debiased classifier from biased classifier. In *Advances in Neural Information Processing Systems*, 2020.
- [62] A. Bielski and P. Favaro. Emergence of object segmentation in perturbed generative models. In *Advances in Neural Information Processing Systems*, 2019.
- [63] R. Arandjelović and A. Zisserman. Object discovery with a copy-pasting gan. *arXiv preprint arXiv:1905.11369*, 2019.
- [64] D. T. Nguyen, M. Dax, C. K. Mummadi, T. P. N. Ngo, T. H. P. Nguyen, Z. Lou, and T. Brox. Deepusps: Deep robust unsupervised saliency prediction with self-supervision. In *Advances in Neural Information Processing Systems*, 2019.
- [65] J. Zhang, T. Zhang, Y. Dai, M. Harandi, and R. Hartley. Deep unsupervised saliency detection: A multiple noisy labeling perspective. In *IEEE Conference on Computer Vision and Pattern Recognition*, 2018.
- [66] D. Zhang, J. Han, and Y. Zhang. Supervision by fusion: Towards unsupervised learning of deep salient object detector. In *IEEE International Conference on Computer Vision*, 2017.
- [67] A. Voynov, S. Morozov, and A. Babenko. Big gans are watching you: Towards unsupervised object segmentation with off-the-shelf generative models. *arXiv preprint arXiv:2006.04988*, 2020.
- [68] A. Brock, J. Donahue, and K. Simonyan. Large scale gan training for high fidelity natural image synthesis. In *International Conference on Learning Representations*, 2019.
- [69] M. Engelcke, O. P. Jones, and I. Posner. Genesis-v2: Inferring unordered object representations without iterative refinement. *arXiv preprint arXiv:2104.09958*, 2021.
- [70] P. Goyal, M. Caron, B. Lefauveux, M. Xu, P. Wang, V. Pai, M. Singh, V. Liptchinsky, I. Misra, A. Joulin, et al. Self-supervised pretraining of visual features in the wild. *arXiv preprint arXiv:2103.01988*, 2021.
- [71] Y. Tian, O. J. Henaff, and A. v. d. Oord. Divide and contrast: self-supervised learning from uncurated data. *arXiv preprint arXiv:2105.08054*, 2021.
- [72] D. C. Liu and J. Nocedal. On the limited memory bfgs method for large scale optimization. *Mathematical programming*, 1989.
- [73] L. Van der Maaten and G. Hinton. Visualizing data using t-sne. *Journal of machine learning research*, 2008.

## A Algorithms

---

**Algorithm 1** PyTorch-style pseudo-code for the Iterative ContraCAM.

---

```
# input: image (b, c, h, w)

masked_image = image # initial: original image

queues = []
for i in n_iters:
    feature = get_features(masked_image) # spatial features
    feature.requires_grad = True
    output = get_projection(feature) # projection outputs

    if i == 0:
        key = output.detach() # original images
        queues.append(output.detach()) # masked images

    score = contrastive_score(output, key, queues) # See Algorithm 2
    cam = compute_cam(feature, score, size=(h, w)) # See Algorithm 3

    mask = max(mask, cam) if i > 0 else cam # union over iterations
    masked_image = image * (1 - mask) + mask_color * mask # soft mask

return mask
```

---

---

**Algorithm 2** PyTorch-style pseudo-code for the contrastive score.

---

```
# input: query (b,d), key (b,d), queues List[(b,d)]

pos = einsum('nc,nc->n', [query, key])
neg = cat([einsum('nc,kc->nk', [query, q]) * (1 - query.size(0))
          for q in queues], dim=1)

score = (pos.exp().sum(dim=1) / neg.exp().sum(dim=1)).log()
return score
```

---

---

**Algorithm 3** PyTorch-style pseudo-code for the Class Activation Map (CAM).

---

```
# input: feature (b,c,h,w), score (b), size=(H,W)

grad = autograd.grad(score.sum(), feature)[0]

weight = adaptive_avg_pool2d(grad, output_size=(1, 1))
weight = weight.clamp_min(0) # clamp negative weights

cam = sum(weight * feature, dim=1, keepdim=True).detach() # weighted sum
cam = interpolate(cam, size=(H,W)) # scale-up to image size
cam = normalize(relu(cam)) # normalize to [0,1]
return cam
```

---

## B Implementation details

We build our code upon the PyTorch [52] and PyTorch Lightning<sup>6</sup> library. Further implementation details and additional libraries for each experiment are stated in the remaining subsections.

### B.1 Implementation details for object localization results

We train MoCov2 under the ResNet-18 architecture on CUB, Flowers, COCO, and ImageNet-9 datasets for the segmentation results. We train the models with batch size 256, COCO, and ImageNet-9 for 800 epochs and CUB and Flowers for 2,000 epochs since the latter has few samples. We follow the augmentations of He et al. [1]: color jitter with strength (0.4,0.4,0.4,0.1), random grayscale with probability 0.2, and Gaussian blur with kernel size 23 and standard deviation sampled from (0.1,2.0) with probability 0.5; except random crop patches with size (0.08,1.0) instead of the original (0.2,1.0) as it performed better for images with small objects. We use a learning rate of 0.03 with a cosine annealing schedule. These training configurations are applied for all experiments.

We apply the expansion trick [47]: doubly expand the resolution of penultimate spatial activations by decreasing the stride of the convolutional layer in the final residual block to detect small objects with CAM. Note that we only apply this trick at inference time and do not change the training; namely, the model is trained with the original  $7 \times 7$  resolution but inferred with the expanded  $14 \times 14$  of the spatial activations. We also tried training the models using the modified  $14 \times 14$  resolution but did not see much gain. We run ten iterations for the Iterative ContraCAM and apply the conditional random field following the default hyperparameters<sup>7</sup> from the pydensecrf library [48]. We report the mask mean intersection-over-union (mIoU) between the predicted and ground-truth segmentation masks.

For the comparison of the classifier CAM and ContraCAM, we use the publicly available supervised classifier<sup>8</sup> and MoCov2<sup>9</sup> trained on the ImageNet dataset under the ResNet-50 architecture. Here, we do not apply the expansion trick and run a single iteration for the ContraCAM. We report the MaxBoxAccV2 [47]: averages the ratios of the bounding boxes whose mean intersection-over-unions (mIoUs) are larger than 30%, 50%, and 70% where the boxes for each mIoU percentages are generated by the CAM binarized by the optimal thresholds, on the ImageNet, CUB, Flowers, VOC, and OpenImages dataset following the official evaluation code.<sup>10</sup> Recall that we report the transfer performance of the predicted CAMs from the ImageNet-trained models for these experiments.

### B.2 Implementation details for contextual bias results

We train MoCov2 and BYOL under the ResNet-18 and ResNet-50 architectures on the COCO dataset for 800 epochs with batch size 256. We extract the bounding boxes from the binarized CAM masks using the `findContours` function in the OpenCV library [49]. We compute the boxes with MoCov2 trained on ResNet-18 and ResNet-50 architectures and use them for the debiased MoCov2 and BYOL using the same architectures. We found that giving some margin for the boxes slightly improves the performance by observing more object boundaries. Specifically, we expand the boxes with 20% of margins (width for left-and-right and height for up-and-down) found from the experiments using the ground-truth boxes and use the same margins for the CAM boxes. We also remove the small boxes, specifically smaller than 1% of the image size, to remove vague low-resolution objects.

We follow the linear evaluation scheme of Chen et al. [2]: train a  $\ell_2$ -regularized multinomial logistic regression classifier on top of the pre-computed representation using the L-BFGS [72] optimizer. We compute the representation with the center cropped images and choose the  $\ell_2$ -regularization parameter from  $(10^{-6}, 10^5)$  spaced with a range of 45 logarithmically. We evaluate the transfer performance on the COCO-Crop (crop objects of the COCO dataset with 20% of margins), CIFAR-10, CIFAR-100, CUB, Flowers, Food, and Pets datasets using the linear classifier trained and tested on each dataset. For detection experiments, we follow the fine-tuning configuration of He et al. [1] evaluated on the COCO dataset. We use the Detectron<sup>11</sup> library for the detection experiments.

<sup>6</sup><https://github.com/PyTorchLightning/pytorch-lightning>

<sup>7</sup><https://github.com/lucasb-eyer/pydensecrf>

<sup>8</sup><https://pytorch.org/vision/stable/models.html>

<sup>9</sup><https://github.com/facebookresearch/moco>

<sup>10</sup><https://github.com/clovaai/wsolevaluation>

<sup>11</sup><https://github.com/facebookresearch/Detectron>

### B.3 Implementation details for background bias results

We provide the visual examples of the Background Challenge [23] in Figure 5 and distribution-shifted datasets of ImageNet [51]: ImageNet-Sketch [29], Stylized-ImageNet [39], ImageNet-R [40], and ImageNet-C [30] datasets in Figure 6. We train the models on the ImageNet-9 [23], i.e., the ORIGINAL dataset of the Background Challenge, which contains 9 superclass (370 class) of the full ImageNet for both background and distribution shifts experiments. Thus, we use the the corresponding 9 superclass subsets of the distribution-shifted datasets, denoted by putting ‘-9’ at the suffix of the dataset names.

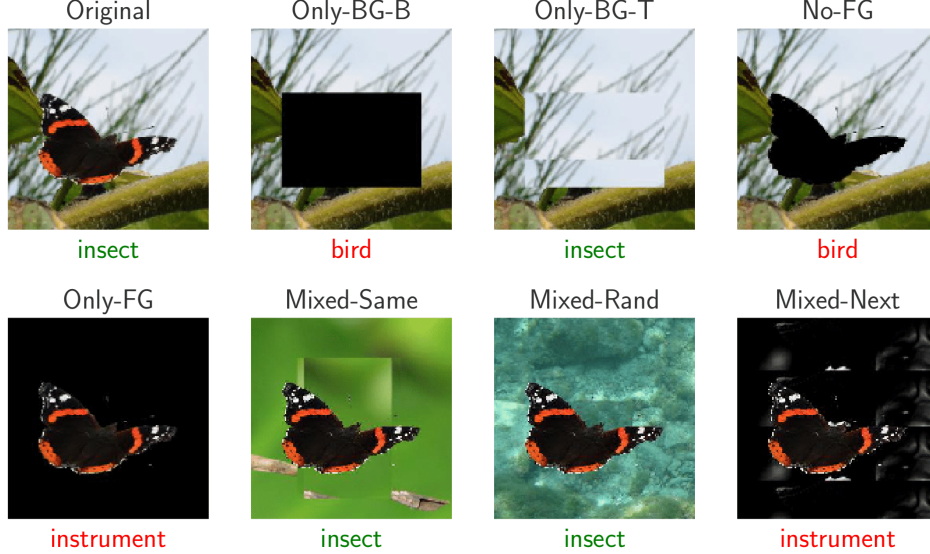


Figure 5: Visual examples of the Background Challenge [23]. Image from the original paper.



(a) ImageNet-Sketch [29] (b) Stylized-ImageNet [39] (c) ImageNet-R [40] (d) ImageNet-C [30]

Figure 6: Visual examples of the distribution-shifted datasets of ImageNet [51] for ‘dog’ class.

We train MoCov2 and BYOL under the ResNet-18 architecture on the ORIGINAL dataset of the Background Challenge for 800 epochs with batch size 256. We use the ContraCAM masks from MoCov2 to train debiased MoCov2 and BYOL for debiased BYOL. We threshold the CAM values with a threshold of 0.2 to find the largest contour, find the largest rectangle outside the contour to create the background patch and tile it for the background-only image. We train a linear classifier on the ORIGINAL dataset and evaluate test accuracy on the Background Challenge and distribution-shifted ImageNet 9 superclass subsets for the background and distribution shift results.

## C Additional localization results

### C.1 Visualization of ContraCAM without negative signal removal

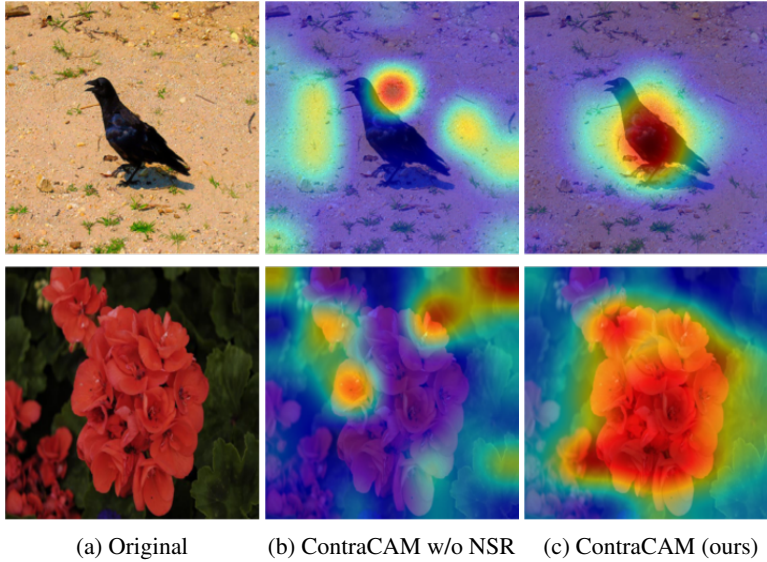


Figure 7: Visualization of ContraCAM without negative signal removal (NSR).

Figure 7 shows the examples of ContraCAM without negative signal removal. The negative signals from similar objects in different images disturb the localization results by canceling positive signals; spread in random locations. Therefore, removing these signals improves the localization results.

### C.2 Ablation study on the number of iterations

Table 7: Mask mIoU of ContraCAM with various number of iterations.

Iteration	CUB	Flowers	COCO	ImageNet-9
1	0.249	0.374	0.081	0.090
2	0.402	0.662	0.182	0.220
3	0.447	0.738	0.256	0.328
5	<b>0.461</b>	0.753	0.308	0.417
10	0.460	<b>0.776</b>	<b>0.319</b>	<b>0.427</b>
20	0.458	0.737	0.318	0.419

We present the ablation study on the number of iterations for the ContraCAM in Table 7. One needs a sufficient number of iterations (e.g., 5) since too small numbers of iterations often detect subregions or miss some objects. Also, note that the CAM shows stable results for large numbers (e.g., 20) of iterations and converges to some stationary values, though it slightly harms the best value of 10.

### C.3 Ablation study on the choice of negative batch

We study the effects of the negative batch for the ContraCAM. Recall that the ContraCAM finds the most discriminative regions compared to the negative batch; it assumes that images have similar backgrounds but different objects. For a sanity check, we construct a negative batch containing similar objects. Figure 8 shows an example of the ContraCAM using a giraffe-only and random batch as the negatives. ContraCAM highlights background when compared to the giraffe-only batch.

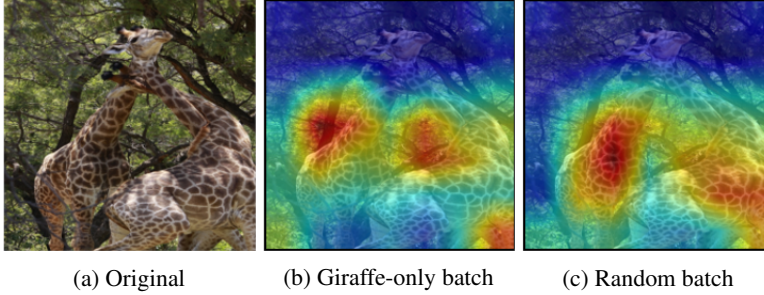


Figure 8: Visualization of the similar-objects and random negative batches.

However, the pathological selection of the negative batch rarely occurs in practice; using a small number of random samples can alleviate the issue. Table 8 shows the effects of the negative batch size for the ContraCAM. Using a small batch (e.g., of size 4) almost match the performance of the larger batch (e.g., of size 64). We use the random batch of size 64 for all our experiments.

Table 8: Mask mIoU of ContraCAM with various negative batch sizes.

Batch size	CUB	Flowers	COCO	ImageNet-9
4	0.451	0.731	0.315	0.428
16	0.455	0.731	0.317	<b>0.429</b>
64	<b>0.460</b>	<b>0.776</b>	<b>0.319</b>	0.427

#### C.4 Comparison with the Classifier CAM

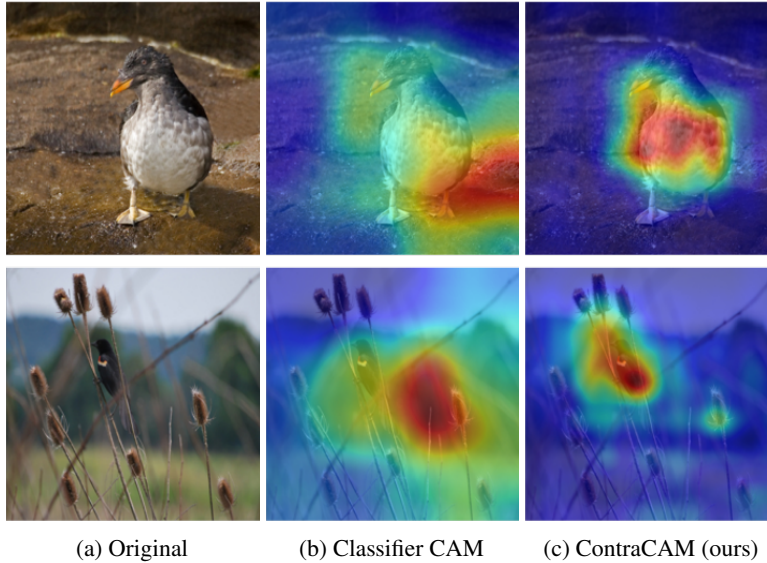


Figure 9: Visualization of the Classifier CAM and ContraCAM.

Table 9: MaxBoxAccV2 of the Classifier CAM and ContraCAM using the supervised classifier and MoCov2 trained on the ImageNet dataset under the ResNet-50 architecture. Res $\times$ 2 denotes the usage of the double expansion trick [47] of the resolution of penultimate spatial activations.

Model	Method	Res $\times$ 2	ImageNet	CUB	Flowers	VOC	OpenImages
Supervised	Classifier CAM		55.95	55.52	76.87	53.88	48.01
Supervised	Classifier CAM	✓	55.01	43.23	73.31	52.27	47.23
MoCov2	Classifier CAM		57.79	63.84	74.29	59.45	51.99
MoCov2	Classifier CAM	✓	60.04	62.87	78.01	61.03	53.06
MoCov2	ContraCAM (ours)		54.57	60.33	74.29	58.64	48.84
MoCov2	ContraCAM (ours)	✓	55.88	64.07	75.64	59.40	49.89

We compare the ContraCAM and classifier CAM under the publicly available supervised classifier and MoCov2 trained on the ImageNet dataset. Somewhat interestingly, the ContraCAM often outperforms the classifier CAM on the transfer setting, e.g., when transferred to the CUB dataset, as shown in Figure 9. This is because some samples of the CUB dataset are out-of-class of the ImageNet, and the classifier fails to understand the important features unrelated to the original classes.

To check whether the superiority of the ContraCAM comes from the score function or better backbone, we also train a linear classifier on top of the MoCov2 backbone using the ImageNet dataset and test the classifier CAM. Table 9 shows that the ContraCAM on MoCov2 even outperforms the classifier CAM on the same backbone for the ImageNet to CUB transfer scenario.

On the other hand, the table shows that the double expansion trick [47] of the resolution of penultimate spatial activations is more effective for MoCov2 while degrading the supervised classifier; MoCov2 is trained with stronger augmentations, making CAM robust to the modification of the architecture. Thus, we only apply the expansion trick for the MoCov2 results in Table 2.

### C.5 Comparison with the gradient-based saliency methods

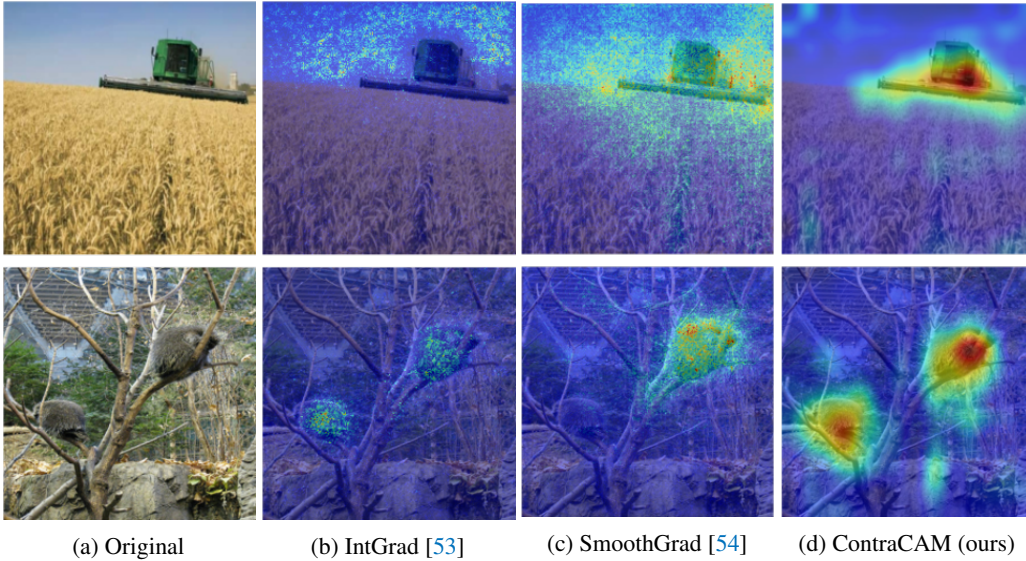


Figure 10: Visualization of various saliency methods using the contrastive score Eq. (1).

Table 10: MaxBoxAccV2 of various saliency methods using the contrastive score Eq. (1). We compute the saliencies from the MoCov2 trained on the ImageNet dataset under the ResNet-50 architecture.

Method	ImageNet	CUB	Flowers	VOC	OpenImages
IntGrad [53]	48.40	35.44	70.73	48.52	49.48
SmoothGrad [54]	51.70	51.50	72.83	57.26	48.67
ContraCAM (ours)	<b>55.88</b>	<b>64.07</b>	<b>75.64</b>	<b>59.40</b>	<b>49.89</b>

We compare the ContraCAM and gradient-based saliency methods using the contrastive score Eq. (1). All methods use the same score function but only differ from localization: the weighted sum of activations (i.e., CAM) or directly propagate the gradients to the input space (i.e., gradient-based saliencies). We choose two representative gradient-based saliency methods: Integrated Gradients (IntGrad) [53] and SmoothGrad [54], which ensembles multiple gradients for better saliency detection. Specifically, IntGrad ensembles the gradients of the linear interpolation of the image and the zero image, and SmoothGrad ensembles the gradients of the image added by random Gaussian noises. We average ten gradients, either interpolation or Gaussian noises, for both methods.

Figure 10 and Table 10 present the visual examples and quantitative results measured by MaxBox-AccV2, respectively. The gradient-based saliencies provide sparse points as outputs, which can be hard to aggregate as segmentation masks. In contrast, ContraCAM provides smooth maps which are more interpretable and easily used for applications, e.g., post-process to bounding boxes. Furthermore, the gradient-based saliencies detect larger regions than ContraCAM. We think it is due to the negative signals: unlike ContraCAM, it is non-trivial to remove them for the gradient-based saliencies.

## D Additional contextual bias results

### D.1 Hard negative issue in MoCov2

We found that MoCov2 trained with the object-aware random crop (OA-Crop) using ground-truth (GT) bounding boxes does not perform well, often worse than the original image (Baseline). This is because the contrastive learning objective is hard to optimize and unstable during training for the OA-Crop (GT), as shown in Figure 11. In contrast, OA-Crop using the ContraCAM boxes is much stable, yet it is a little harder to optimize than the original image.

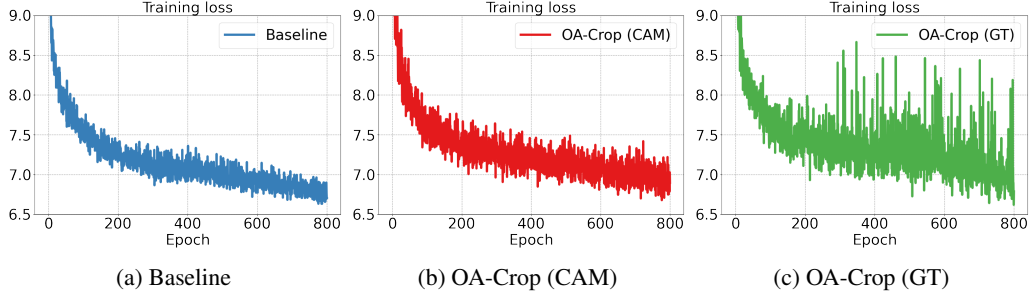


Figure 11: Training loss curve of MoCov2 trained under the COCO dataset.

The reason behind this phenomenon is that the ground-truth boxes often contain objects that are hard to distinguish from each other, i.e., hard negatives for contrastive learning. In contrast, ContraCAM finds more discriminative objects as defined in Eq. (1). Figure 12 shows the histogram of the number of ContraCAM and ground-truth boxes, and Figure 13 shows a visual example of them. ContraCAM finds the most recognizable 1~3 objects from the full ground-truth boxes.

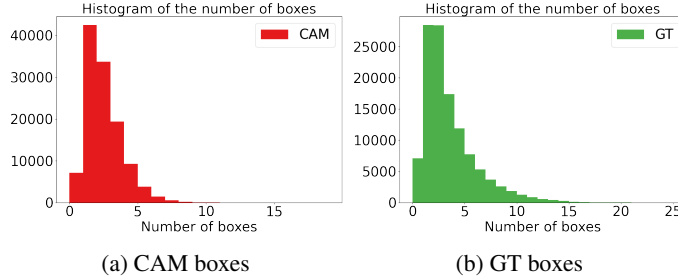


Figure 12: Histogram of the number of ContraCAM and ground-truth boxes.

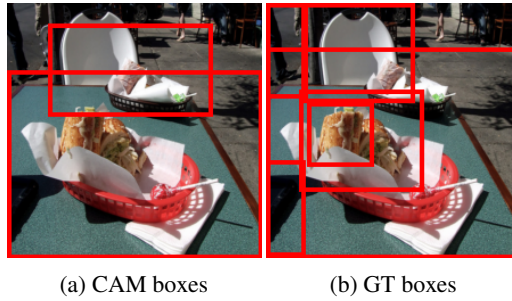


Figure 13: Visualization of the ContraCAM and ground-truth boxes.

## D.2 Analysis on the contextual bias

We analyze whether the object-aware random crop (OA-Crop) actually relieves the contextual bias. To verify this, we visualize the embeddings of correlated classes under the original MoCov2 and the debiased model using the OA-Crop with the ContraCAM boxes. Specifically, we choose giraffe and zebra, which frequently co-occurs in the safari scene (see Figure 1a). Figure 14 shows the t-SNE [73] visualization of the giraffe and zebra embeddings of the original and debiased models. The debiased OA-Crop (CAM) model less entangles the features of giraffe and zebra. However, even the debiased model using the ground-truth boxes, i.e., OA-Crop (GT), does not perfectly disentangle the features; since the bounding boxes often contain nearby or occluded objects.

We also quantitatively measure the contextual bias of the models in Table 11. Specifically, we compute the average minimum  $\ell_2$ -distance of the features, i.e.,

$$\frac{1}{|\mathcal{X}|} \sum_{x \in \mathcal{X}} \min_{y \in \mathcal{Y}} d(x, y) + \frac{1}{|\mathcal{Y}|} \sum_{y \in \mathcal{Y}} \min_{x \in \mathcal{X}} d(x, y), \quad (5)$$

where  $\mathcal{X}, \mathcal{Y} \subset \mathcal{R}^m$  are the penultimate embeddings of each class (giraffe and zebra) and  $d$  denotes a  $\ell_2$ -distance function, under the MoCov2 using the ResNet-50 architecture. The model trained by OA-Crop (CAM) has a larger distance between the embeddings than the original image.

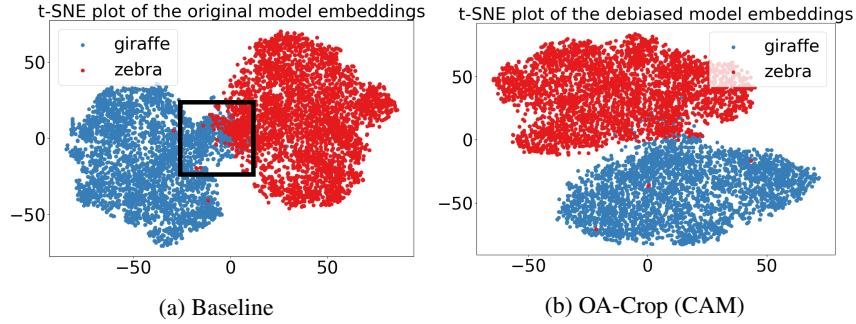


Figure 14: t-SNE [73] visualization of the giraffe and zebra embeddings.

Table 11: Average minimum  $\ell_2$ -distance of giraffe and zebra embeddings.

Baseline	OA-Crop (CAM)	OA-Crop (GT)
0.2441	0.2790	0.3824

### D.3 Class-wise accuracy on CIFAR-10

Table 12: Class-wise linear evaluation (%) of MoCov2 and BYOL on CIFAR-10 under the ResNet-50 architecture, following the setting of Table 3. OA-Crop is not biased to the certain classes.

Model	OA-Crop	Airplane	Automobile	Bird	Cat	Deer	Dog	Frog	Horse	Ship	Truck
MoCov2	-	79.5	86.9	67.2	61.6	74.0	68.1	82.1	79.2	89.4	87.8
MoCov2	CAM	88.9 (+9.4)	92.8 (+5.9)	74.8 (+7.6)	70.0 (+8.4)	78.6 (+4.6)	76.6 (+8.5)	88.6 (+6.5)	85.1 (+5.9)	93.8 (+4.4)	91.8 (+4.0)
MoCov2	GT	89.0 (+9.5)	94.0 (+7.1)	76.5 (+9.3)	70.9 (+9.3)	78.2 (+4.2)	73.9 (+5.8)	87.0 (+4.9)	86.5 (+7.3)	92.5 (+3.1)	91.8 (+4.0)
BYOL	-	78.6	87.8	64.1	62.3	68.8	68.4	83.8	78.7	87.2	86.8
BYOL	CAM	86.2 (+7.6)	93.2 (+5.4)	73.4 (+9.3)	69.4 (+7.1)	76.2 (+7.4)	74.7 (+6.3)	87.5 (+3.7)	83.6 (+4.9)	92.1 (+4.9)	91.6 (+4.8)
BYOL	GT	90.2 (+11.6)	94.6 (+6.8)	76.7 (+12.6)	73.0 (+10.7)	80.1 (+11.3)	79.8 (+11.4)	89.4 (+5.6)	88.6 (+9.9)	93.6 (+6.4)	93.2 (+6.4)

We check if our debiased models suffer from the over-reliance on conspicuous objects as concerned in the potential negative effects section. Table 12 shows the class-wise accuracy of the original and our debiased models on CIFAR-10. OA-Crop does not degrade the performance on certain classes, implying that the concerned bias issue does not occur for our considered transfer scenario.

### D.4 Second iteration using the CAM from the debiased models

Table 13: Linear evaluation (%) of MoCov2 and BYOL on various image classification tasks under the ResNet-18 architecture, following the setting of Table 3. We compare the models trained with the ContraCAM inferred from the original models (Iter. 1) and debiased models (Iter. 2).

Model	OA-Crop	Iter.	Test dataset						
			COCO-Crop	CIFAR10	CIFAR100	CUB	Flowers	Food	Pets
MoCov2	-	-	67.38	66.83	41.85	15.36	58.81	45.88	45.37
MoCov2	CAM	1	69.92 (+2.54)	76.73 (+9.90)	53.25 (+11.40)	16.26 (+0.90)	64.77 (+5.96)	48.56 (+2.68)	47.37 (+2.00)
MoCov2	CAM	2	68.53 (+1.15)	76.54 (+9.71)	52.64 (+10.79)	16.62 (+1.26)	64.89 (+6.08)	47.34 (+1.46)	46.77 (+1.40)
BYOL	-	-	67.74	67.82	41.96	17.24	64.79	49.58	52.90
BYOL	CAM	1	70.85 (+3.11)	77.37 (+9.55)	54.79 (+12.83)	18.24 (+1.00)	70.56 (+5.77)	53.16 (+3.58)	54.27 (+1.37)
BYOL	CAM	2	70.96 (+3.22)	77.62 (+9.80)	54.78 (+12.82)	20.14 (+2.90)	71.31 (+6.52)	53.38 (+3.80)	53.50 (+0.60)

We compare the models trained with the ContraCAM inferred from the original models (Iter. 1) and the debiased models (Iter. 2) in Table 13. Using the debiased models has no additional gain from the original models. Thus, we use the single iteration version for all experiments.

### D.5 Comparison with the ImageNet-trained models

Table 14: Linear evaluation (%) of MoCov2 and BYOL on various image classification tasks under the ResNet-18 architecture, following the setting of Table 3. We additionally compare with the models trained under the 10% subset of the ImageNet dataset (i.e., ImageNet 10%).

Model	Dataset	OA-Crop	Test dataset						
			COCO-Crop	CIFAR10	CIFAR100	CUB	Flowers	Food	Pets
MoCov2	COCO	-	67.38	66.83	41.85	15.36	58.81	45.88	45.37
MoCov2	COCO	CAM	69.92	76.73	53.25	16.26	64.77	48.56	47.37
MoCov2	COCO	GT	71.60	77.99	53.32	18.19	65.43	46.41	48.68
MoCov2	ImageNet 10%	-	66.28	75.28	48.64	23.75	67.99	48.70	64.16
BYOL	COCO	-	67.74	67.82	41.96	17.24	64.79	49.58	52.90
BYOL	COCO	CAM	70.85	77.37	54.79	18.24	70.56	53.16	54.27
BYOL	COCO	GT	76.59	81.23	58.11	22.99	73.25	55.33	59.80
BYOL	ImageNet 10%	-	68.96	78.51	55.40	29.89	78.14	55.10	70.16

We compare the models trained under the COCO dataset (original or with OA-Crop) with the 10% subset of the ImageNet dataset (i.e., ImageNet 10%) under the ResNet-18 architecture in Table 14. We randomly choose 10% of samples to make a similar size ( $\sim 100,000$ ) with the COCO dataset. While the models trained under COCO performing better on the COCO-Crop, ImageNet significantly outperforms the other datasets, implying ImageNet has fewer distributional shifts with them.

## E Additional background bias results

### E.1 Comparison with the copy-and-paste augmentation

Table 15: Test accuracy (%) on background shifts following the setting of Table 5. We compare the background mixup using the ContraCAM (BG-Mixup) and the copy-and-paste version using the binarized CAM (BG-HardMix). Bold denotes the best results among the same model.

Dataset	MoCov2			BYOL		
	Baseline	BG-Mixup (CAM)	BG-HardMix (CAM)	Baseline	BG-Mixup (CAM)	BG-HardMix (CAM)
Original $\uparrow$	89.17 $\pm$ 0.49	<b>90.73</b> $\pm$ 0.05 (+1.56)	88.96 $\pm$ 0.50 (-0.21)	87.30 $\pm$ 0.61	<b>89.30</b> $\pm$ 0.02 (+2.00)	88.71 $\pm$ 0.28 (+1.41)
Only-BG-B $\downarrow$	31.29 $\pm$ 2.46	<b>29.60</b> $\pm$ 0.89 (-1.69)	31.28 $\pm$ 2.03 (-0.01)	<b>25.59</b> $\pm$ 0.78	25.70 $\pm$ 3.46 (+0.11)	26.67 $\pm$ 1.32 (+1.08)
Only-BG-T $\downarrow$	44.91 $\pm$ 0.16	<b>41.95</b> $\pm$ 0.38 (-2.96)	44.36 $\pm$ 1.40 (-0.55)	42.83 $\pm$ 0.51	<b>39.94</b> $\pm$ 0.52 (-2.89)	42.02 $\pm$ 0.45 (-0.81)
Only-FG $\uparrow$	63.62 $\pm$ 4.71	<b>70.55</b> $\pm$ 1.71 (+6.93)	67.75 $\pm$ 0.89 (+4.13)	61.04 $\pm$ 0.94	<b>67.53</b> $\pm$ 0.30 (+6.49)	63.61 $\pm$ 1.65 (+2.57)
Mixed-Same $\uparrow$	80.98 $\pm$ 0.34	<b>84.13</b> $\pm$ 0.33 (+3.15)	82.19 $\pm$ 0.61 (+1.21)	79.30 $\pm$ 0.31	<b>81.28</b> $\pm$ 0.53 (+1.98)	81.25 $\pm$ 0.48 (+1.95)
Mixed-Rand $\uparrow$	60.34 $\pm$ 0.66	<b>66.89</b> $\pm$ 0.54 (+6.55)	63.46 $\pm$ 0.84 (+3.12)	58.03 $\pm$ 0.85	<b>63.83</b> $\pm$ 0.53 (+5.80)	61.93 $\pm$ 0.17 (+3.90)
Mixed-Next $\uparrow$	55.50 $\pm$ 0.71	<b>63.64</b> $\pm$ 0.41 (+8.14)	59.19 $\pm$ 0.94 (+3.69)	53.35 $\pm$ 0.36	<b>63.05</b> $\pm$ 3.54 (+9.70)	58.13 $\pm$ 1.22 (+4.78)
BG-Gap $\downarrow$	20.64 $\pm$ 0.36	<b>17.24</b> $\pm$ 0.31 (-3.40)	18.73 $\pm$ 0.54 (-1.91)	21.27 $\pm$ 0.64	<b>17.45</b> $\pm$ 0.15 (-3.82)	19.32 $\pm$ 0.42 (-1.95)

We compare the background mixup using the ContraCAM (BG-Mixup) with the copy-and-paste augmentation using the binarized CAM (BG-HardMix) in Table 15. BG-Mixup (CAM) shows better accuracy (e.g., ORIGINAL) and better generalization (e.g., MIXED-RAND) than the BG-HardMix, implying that the soft blending of foreground and background images performs better than the hard copy-and-paste. Indeed, one should consider the confidence of the predicted CAM masks as they are inaccurate. Also, the soft blending gives a further regularization effect of mixup [41].

### E.2 Ablation study on the mixup probability

Table 16: Test accuracy (%) on background shifts following the setting of Table 5. We study the effect of the mixup probability  $p_{\text{mix}}$ . Bold denotes the best results among the same model.

Model	$p_{\text{mix}}$	Test dataset							
		Original $\uparrow$	Only-BG-B $\downarrow$	Only-BG-T $\downarrow$	Only-FG $\uparrow$	Mixed-Same $\uparrow$	Mixed-Rand $\uparrow$	Mixed-Next $\uparrow$	BG-Gap $\downarrow$
MoCov2	0.0	88.67	28.47	44.99	58.25	81.21	60.57	56.22	20.64
MoCov2	0.2	90.52 (+1.85)	<b>26.32</b> (-2.15)	43.73 (-1.26)	69.01 (+10.76)	82.91 (+1.70)	64.89 (+4.32)	62.12 (+5.90)	18.02 (-2.62)
MoCov2	0.3	<b>91.09</b> (+2.42)	31.53 (+3.06)	42.91 (-2.08)	68.42 (+10.17)	84.25 (+3.04)	66.72 (+6.15)	63.68 (+7.46)	17.53 (-3.11)
MoCov2	0.4	90.72 (+2.05)	28.69 (+0.22)	<b>42.05</b> (-2.94)	<b>72.35</b> (+14.10)	<b>84.42</b> (+3.21)	<b>67.51</b> (+6.94)	64.04 (+7.82)	<b>16.91</b> (-3.73)
MoCov2	0.5	90.81 (+2.14)	30.07 (+1.60)	42.20 (-2.79)	68.96 (+10.71)	83.26 (+2.05)	66.27 (+5.70)	<b>64.15</b> (+7.93)	16.99 (-3.65)
BYOL	0.0	86.72	26.32	43.41	60.22	78.96	57.11	53.01	21.85
BYOL	0.2	88.40 (+1.68)	22.72 (-3.60)	41.38 (-2.03)	63.78 (+3.56)	<b>81.53</b> (+2.57)	62.86 (+5.75)	59.09 (+6.08)	18.67 (-3.18)
BYOL	0.3	<b>89.31</b> (+2.59)	<b>22.47</b> (-3.85)	<b>39.68</b> (-3.73)	67.36 (+7.14)	80.89 (+1.93)	<b>63.58</b> (+6.47)	<b>61.01</b> (+8.00)	<b>17.31</b> (-4.54)
BYOL	0.4	88.47 (+1.75)	29.04 (+2.72)	40.77 (-2.64)	66.20 (+5.98)	81.33 (+2.37)	62.77 (+5.66)	59.09 (+6.08)	18.56 (-3.29)
BYOL	0.5	88.02 (+1.30)	29.48 (+3.16)	40.20 (-3.21)	<b>69.09</b> (+8.87)	<b>81.53</b> (+2.57)	62.40 (+5.29)	59.04 (+6.03)	19.13 (-2.72)

We study the effect of the mixup probability  $p_{\text{mix}}$ , a probability of applying BG-Mixup augmentation. Table 16 shows the BG-Mixup results with varying  $p_{\text{mix}} \in \{0.2, 0.3, 0.4, 0.5\}$  applied on MoCov2 and BYOL. We first remark that BG-Mixup gives a consistent gain regardless of  $p_{\text{mix}}$ . Despite of the insensitivity on the hyperparameter  $p_{\text{mix}}$ , we choose  $p_{\text{mix}} = 0.4$  for MoCov2 and  $p_{\text{mix}} = 0.3$  for BYOL since they performed best for the most datasets in Background Challenge. MoCov2 permits the higher mixup probability since finding the closest sample from the finite batch (i.e., contrastive learning) is easier than clustering infinitely many samples (i.e., positive-only methods).

### E.3 ContraCAM vs. GT masks on the distribution shifts

Table 17: Test accuracy (%) on distribution shifts following the setting of Table 6. We compare the copy-and-paste version using the ground-truth masks (BG-HardMix (GT)) and the background mixup using the ContraCAM masks (BG-Mixup (CAM)). Bold denotes the best results.

Model	Augmentation	Test dataset			
		ImageNet-Sketch-9	Stylized-ImageNet-9	ImageNet-R-9	ImageNet-C-9
MoCov2	Baseline	46.70 $\pm$ 0.67	25.66 $\pm$ 0.54	37.51 $\pm$ 0.80	31.82 $\pm$ 0.40
MoCov2	+BG-HardMix (GT)	51.60 $\pm$ 0.91 (+4.90)	29.95 $\pm$ 2.64 (+4.09)	40.15 $\pm$ 0.34 (+3.39)	31.45 $\pm$ 1.20 (-0.37)
MoCov2	+BG-Mixup (CAM)	<b>52.15</b> $\pm$ 0.93 (+5.45)	<b>33.36</b> $\pm$ 0.61 (+7.70)	<b>41.50</b> $\pm$ 0.45 (+3.99)	<b>44.39</b> $\pm$ 0.89 (+12.57)
BYOL	Baseline	45.15 $\pm$ 1.12	23.80 $\pm$ 0.45	36.21 $\pm$ 0.31	28.62 $\pm$ 0.06
BYOL	+BG-HardMix (GT)	51.57 $\pm$ 1.68 (+6.42)	26.72 $\pm$ 0.38 (+2.92)	<b>40.09</b> $\pm$ 0.41 (+3.88)	31.04 $\pm$ 0.52 (+2.42)
BYOL	+BG-Mixup (CAM)	<b>52.40</b> $\pm$ 0.70 (+7.25)	<b>27.01</b> $\pm$ 0.74 (+3.21)	39.62 $\pm$ 0.21 (+3.41)	<b>33.83</b> $\pm$ 0.28 (+5.21)

We provide distribution shift results of the copy-and-paste augmentation using ground-truth masks (BG-HardMix (GT)) in Table 17. BG-HardMix also improves the performance on distribution shifts by enforcing object-centric learning, but BG-Mixup performs better due to both object-centricness and input interpolation. Recall that BG-HardMix (GT) uses ground-truth masks and thus performs better for background shifts; yet, BG-Mixup is better for the distribution shifts.

### E.4 Mixup and CutMix on the background shifts

Table 18: Test accuracy (%) on background shifts following the setting of Table 5. We additionally compare with the Mixup and CutMix. Bold denotes the best results.

Model	Augmentation	Test dataset							
		Original $\uparrow$	Only-BG-B $\downarrow$	Only-BG-T $\downarrow$	Only-FG $\uparrow$	Mixed-Same $\uparrow$	Mixed-Rand $\uparrow$	Mixed-Next $\uparrow$	BG-Gap $\downarrow$
MoCov2	Baseline	89.17	31.29	44.91	63.62	80.98	60.34	55.50	20.64
MoCov2	+Mixup [41]	88.51 (-0.66)	<b>28.54</b> (-2.75)	44.41 (-0.50)	69.53 (+5.91)	80.85 (-0.13)	60.68 (+0.34)	57.25 (+1.75)	20.17 (-0.47)
MoCov2	+CutMix [42]	88.72 (-0.45)	32.47 (+1.18)	47.99 (+3.08)	63.76 (+0.14)	81.48 (+0.50)	59.05 (-1.29)	53.75 (-1.75)	22.43 (+1.79)
MoCov2	+BG-Mixup (ours)	<b>90.73</b> (+1.56)	29.60 (-1.69)	<b>41.95</b> (-2.96)	<b>70.55</b> (+6.93)	<b>84.13</b> (+3.15)	<b>66.89</b> (+6.55)	<b>63.64</b> (+8.14)	<b>17.24</b> (-3.40)
BYOL	Baseline	87.30	<b>25.59</b>	42.83	61.04	79.3	58.03	53.35	21.27
BYOL	+Mixup [41]	85.70 (-1.60)	25.95 (+0.36)	41.00 (-1.83)	61.79 (+0.75)	78.61 (-0.69)	56.27 (-1.76)	51.75 (-1.60)	22.34 (+1.07)
BYOL	+CutMix [42]	86.52 (-0.78)	28.52 (+2.93)	45.88 (+3.05)	61.30 (+0.26)	79.74 (+0.44)	56.46 (-1.57)	51.44 (-1.91)	23.28 (+2.01)
BYOL	+BG-Mixup (ours)	<b>89.30</b> (+2.00)	25.70 (+0.11)	<b>39.94</b> (-2.89)	<b>67.53</b> (+6.49)	<b>81.28</b> (+1.98)	<b>63.83</b> (+5.80)	<b>63.05</b> (+9.70)	<b>17.45</b> (-3.82)

We provide background shift results of Mixup and CutMix in Table 18. Since they are not designed for addressing the background bias, they are not effective on the Background Challenge benchmarks. In contrast, the background mixup is effective on both background and distribution shifts.

### E.5 Corruption-wise results on ImageNet-C-9

We provide the corruption-wise results on the ImageNet-C-9 dataset in Table 19. Background mixup using the ContraCAM masks (BG-Mixup (CAM)) shows the overall best performance. Especially, the BG-Mixup performs well for the ‘weather’ and ‘digital’ class, e.g., improves 24.41% of the baseline to 54.30% (+29.89%), while less performs for the ‘noise’ class. Indeed, the ‘weather’ and ‘digital’ classes require more understanding of the objects (i.e., shape bias) than the ‘noise’ class.

Table 19: Corruption-wise test accuracy (%) on the ImageNet-C-9 dataset. Bold denotes the best results.

Model	Augmentation	Test dataset														
		Noise			Blur			Weather			Digital					
		Gaussian	Shot	Impulse	Defocus	Class	Motion	Zoom	Snow	Frost	Fog	Brightness	Contrast	Elastic	Pixel	JPEG
MoCov2	Baseline	9.24±1.90	9.66±1.65	9.11±1.56	19.32±1.97	19.63±1.55	29.92±1.10	46.42±1.16	43.56±1.98	29.94±0.73	24.41±1.08	72.43±1.80	16.39±1.80	63.64±1.02	25.19±1.82	58.37±1.70
MoCov2	Mixup [41]	18.59±4.42	16.62±3.74	17.9±5.69	19.63±3.76	23.94±6.62	37.17±2.39	50.48±1.44	49.10±2.87	45.11±3.52	32.28±5.57	76.18±0.71	27.10±4.12	65.55±0.36	58.97±0.88	63.59±1.51
MoCov2	CutMix [42]	8.52±3.04	8.51±2.89	8.53±3.01	17.97±5.86	19.12±1.97	32.45±3.09	45.51±1.11	44.82±3.56	30.93±0.51	26.86±1.47	73.24±0.05	16.11±3.15	64.64±2.97	33.85±4.16	53.31±1.87
MoCov2	BG-HardMix (GT)	10.42±1.41	12.54±1.92	10.27±1.24	16.90±0.97	21.49±4.85	31.36±2.50	44.26±1.47	44.08±0.49	29.19±1.34	27.62±3.02	74.18±0.54	14.03±1.05	64.81±1.37	21.28±1.12	49.41±0.53
MoCov2	BG-Mixup (CAM)	31.86±6.58	25.19±4.03	31.42±7.82	20.13±2.05	24.89±3.99	35.92±1.79	49.54±0.36	50.45±1.49	50.56±1.63	54.30±2.35	78.35±0.93	35.76±4.88	65.85±1.16	49.37±4.00	62.25±1.12
BYOL	Baseline	6.50±0.50	7.27±0.78	6.51±0.55	12.54±1.47	18.23±0.45	27.54±3.35	41.57±0.52	36.67±0.69	26.89±1.87	24.42±0.76	69.59±0.56	14.53±0.35	60.55±0.94	20.65±0.72	55.82±1.87
BYOL	Mixup [41]	14.73±4.59	13.85±6.30	13.39±3.57	12.41±1.29	18.48±0.29	26.17±3.00	38.52±1.27	47.55±0.48	34.23±1.39	29.18±3.15	71.33±0.98	12.02±2.44	62.25±0.58	34.39±3.36	58.73±1.12
BYOL	CutMix [42]	7.01±0.55	7.46±0.64	7.26±0.68	12.88±0.31	22.27±2.61	28.71±3.56	42.17±2.75	40.85±0.76	27.24±0.95	26.67±3.33	69.30±0.62	15.03±1.10	62.87±0.37	21.89±1.13	54.17±2.20
BYOL	BG-HardMix (GT)	8.20±0.15	9.43±0.93	7.74±0.44	10.14±1.26	22.97±2.96	26.86±2.71	42.44±1.24	41.38±0.29	32.01±1.10	30.89±1.19	76.58±0.70	16.17±0.92	62.82±0.34	18.24±2.87	59.76±3.69
BYOL	BG-Mixup (CAM)	8.39±1.57	9.20±0.73	7.86±1.76	12.37±0.05	18.55±1.62	26.99±2.97	43.17±2.96	41.48±0.47	35.26±0.40	43.37±2.23	73.24±0.20	20.58±0.77	60.92±0.45	41.51±5.35	64.59±0.58